**MSC**

# The Synthesis and Study of Precious Metal Free Photocatalytic Systems for Proton Reduction to H2.

Oshinowo, Matthew

*Award date:*
2019

*Awarding institution:*
University of York

# *The Synthesis and Study of Precious Metal Free Photocatalytic Systems for Proton Reduction to $H_2$.*

**Masters Research Project**

**By**

**Matthew Oshinowo**

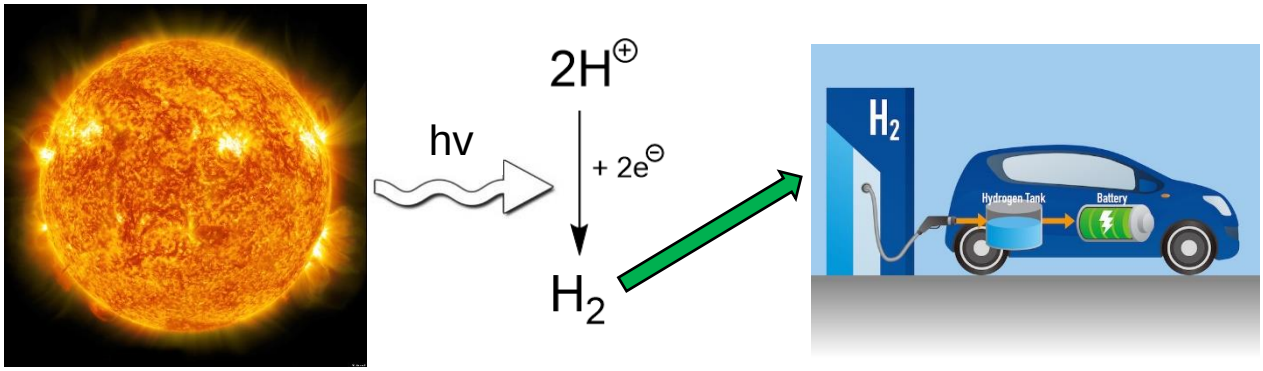


**Supervisors: Dr. Jérôme Fortage, Dr. Marie-Noëlle Collomb, Prof. Robin Perutz.**

**Laboratoire de Chimie Inorganique Redox (CIRE)**

**Département de Chimie Moléculaire (DCM)**

**Université Grenoble Alpes, 38000 Grenoble, France.**

## *Contents*

## *Abbreviations*

| | |
|---|---|
| **14PDN** | $[Co(CR)(H_2O)_2]^{3+}$ |
| **bpy** | 2,2'-bipyridine |
| **CDs** | Cyclodextrins |
| **CV** | Cyclic voltammogram |
| **EY** | Eosin Y |
| **Fl** | Fluorescein |
| **$H_2A$** | Ascorbic acid |
| **$HA^-$** | Ascorbate |
| ***isc*** | Intersystem-crossing |
| **LBI** | 6,6'-bis(ketimino)-2,2'-bipyridine(2,6-diisopropylaniline) |
| **LPI** | 2,9-bis(ketimino)-1,10-phenanthroline(2,6-diisopropylaniline) |
| **MLCT** | Metal-to-ligand charge transfer |
| **OQP** | Oxidative quenching pathway |
| **PS** | Photosensitizer |
| **Ru** | $[Ru(bpy)_3]^{2+}$ |
| **RB** | Rose Bengal |
| **RQP** | Reductive quenching pathway |
| **SD** | Sacrificial electron donor |
| **SCE** | Saturated calomel electrode |
| **$TATA^+$** | Triazatriangulenium cation, $[TATA\text{-}(EE)_3]^+$ |
| **TCS** | Three-component system |
| **TEOA** | Triethanolamine |
| **TEA** | Triethylamine |
| **TOF** | Turn-over-frequency |
| **TON** | Turn-over number |

# A Literature Review of Precious Metal-Free Three-Component Systems for the Reduction of Protons to $H_2$

## *I) Introduction*

It is no secret that our planet is struggling to cope with the effect of our colossal consumption and combustion of fossil fuels. Resources are diminishing at an alarming rate and the vast emissions of $CO_2$ and other greenhouse gases are raising temperatures at a rate that far exceeds the natural one. Consequently, the world is looking towards a clean, green future that would involve the replacement of fossil fuels with a renewable energy source that does not burden the planet. Amongst the renewable energy sources, solar radiation is by far the most plentiful as the solar radiation reaching Earth in one day far exceeds our annual consumption of energy.

If solar energy is to be harnessed for use on a global scale, we need an efficient way of storing, dispatching and releasing this energy on demand. Storing the energy in the chemical bonds of energy carriers, such as molecular hydrogen, is an attractive means of doing this. $H_2$ has the advantage of being 3x more energy dense than petroleum and the only product of its combustion is water.[1] To retrieve the energy in $H_2$ bonds (+286 kJ $mol^{-1}$) hydrogen could be used in fuels cells or directly in internal combustion engines.

Despite the many advantages of a hydrogen economy over a fossil fuel economy, there are many problems that need to be overcome, such as how to generate it. Whilst there are already well-established methods of producing hydrogen from the electrolysis of water using fossil fuel-generated electricity, there are no viable methods for the light-driven splitting of water to form $H_2$ and $O_2$. There are several potential methods of achieving this; photovoltaic, photoelectrochemical, or photothermal devices can be coupled to a water electrolysis device, or it is also possible to directly photocatalytically split water in one device. Photocatalytic water-splitting can be done using semiconductor photoelectrodes, or photochemically in homogeneous aqueous solutions using molecular compounds as 'sacrificial electron donors'.

This review will focus exclusively on the reductive half-equation of water splitting for the formation of $H_2$ via the latter-mentioned method of molecular photocatalytic proton reduction in aqueous solution. This is a very large field of research which has been extensively studied. The review will critically explore this field of research, evaluate some of the key findings that have contributed to achieving a viable photocatalytic system of $H_2$ production, and most importantly, will focus on research that is aiming to do so without the use of rare and expensive precious metals.

## *I) Mechanistic Insight into Proton Reduction*

The late 70's and early 80's saw the development of homogeneous three-component systems (TCS) in an effort to eliminate the use of heterogeneous electrodes, often made from $TiO_2$. The three components include a molecular photosensitizer (PS), a sacrificial electron donor (SD) and a redox catalyst (Cat). Typically, photon absorption by the PS generates an excited state (PS*) which is quenched in either a reductive or oxidative

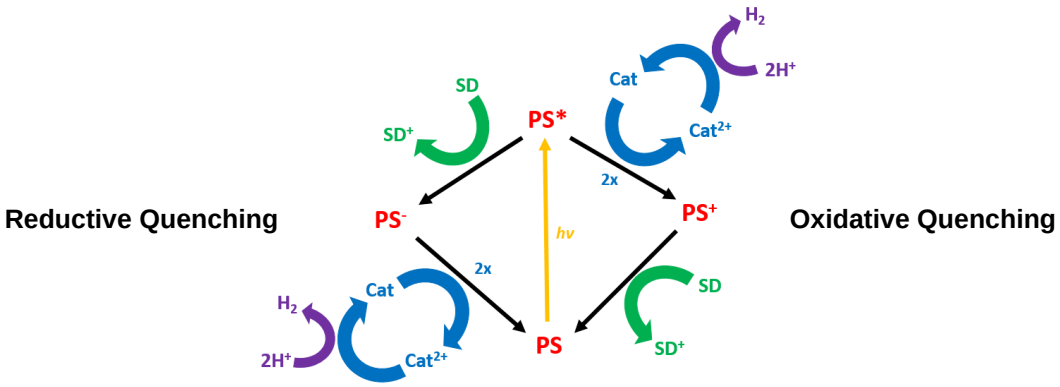


***Figure 1:*** *Mechanism for $H_2$ production in three-component molecular systems via oxidative or reductive quenching.*

quenching pathway (Fig. 1). Reductive quenching proceeds via reduction of PS* to $PS^-$ by the SD, followed by two molecules of $PS^-$ reducing the catalyst to $Cat^{2-}$. Formation of a hydride at the metal centre then leads to formation of $H_2$, the mechanism of which depends on the system. In the oxidative pathway, PS* is firstly oxidised to $PS^+$ by the catalyst before being reduced by the SD back to the ground state.

Being such an active field of research, there are hundreds of PS/Cat combinations used in TCSs. Whilst there are many precious metal-free catalysts, most photosensitizers are complexes that present a rare, often platinum-group metal. As resources of these metals are extremely scarce, alternative photosensitizers need to be found. Organic dyes are currently the best alternative, and as such, this article will review some of the systems that have employed organic dyes as photosensitizers with precious metal-free catalysts. A summary of all the systems reviewed is presented in Table 1.

## *II) A Prototypical Photosensitizer: Tris(bipyridine)ruthenium(II) chloride*

Before reviewing organic dyes, it is first useful to look at the properties of the most commonly used photosensitizer against which all new photosensitizers are compared: tris(bipyridine)ruthenium(II) chloride, $[Ru(bpy)_3]Cl_2$ (denoted **Ru**). Its light-harvesting abilities were first recognised by Demas and Adamson in 1971, before water splitting had been demonstrated.[2] This complex is so widely used owing to its good solubility in water, high absorbance in the visible region, and its good photochemical and redox properties. These properties have been extensively studied and can be found in a useful publication from 1988.[3] **Ru** has a strong absorption coefficient of 14,600 $M^{-1}$ $cm^{-1}$ at 450 nm due to formation of a singlet $^1$MLCT state, i.e. excitation of an electron in a ruthenium $e_g$ orbital to a low-lying $\pi^*$ orbital of a bipyridine ligand. The singlet state then rapidly undergoes *isc* (intersystem-crossing) to the triplet $^3$MLCT state from which electron transfer occurs. The redox potentials demonstrate that ***Ru** is both a better reducing and oxidising agent than **Ru** (Fig. 2).

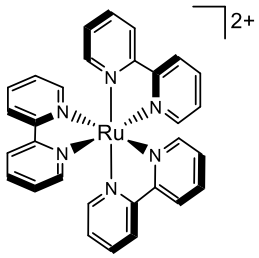


$E_{1/2}$ ($Ru^{2+}/Ru^{+}$) = -1.50 V
$E_{1/2}$ ($Ru^{3+}/Ru^{2+}$) = +1.03 V

$E_{1/2}$ ($*Ru^{2+}/Ru^{+}$) = +0.60 V
$E_{1/2}$ ($Ru^{3+}/*Ru^{2+}$) = -1.07 V

***Figure 2:** Structure and redox potentials of $[Ru(bpy)_3]^{2+}$ (in $H_2O$ vs SCE).*[3]

**Ru** and similar polypyridine-derivatives of ruthenium or other precious metals (mainly iridium, rhenium, or rhodium) have been extensively used over the past few decades. Whilst these complexes are very effective, a move towards organic dyes is needed if these systems are ever to be employed on a large scale. Some of the most commonly used organic photosensitizers are shown in Fig. 3. The common feature of these structures are conjugated arrays of aromatic rings which can easily undergo $\pi$-$\pi^*$ transitions upon absorption of visible light. An efficient photosensitizer must have suitable redox potentials that allow quenching of the excited state by either by the SD or the catalyst.

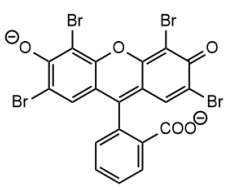


Eosin Y
**(EY)**

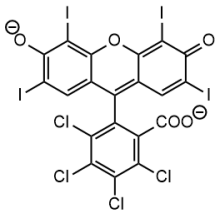


Rose Bengal
**(RB)**

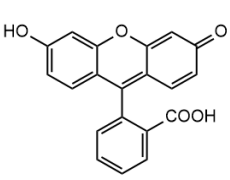


Fluorescein
**(Fl)**

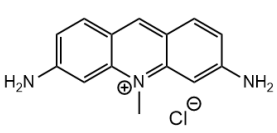


Acriflavine
**(Acr)**

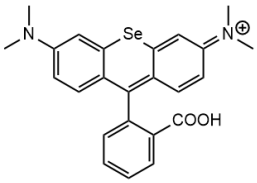


Se-substituted Rhodamine
**(Rhod-Se)**

***Figure 3:** Structures of common organic photosensitizers.*

## *III) Cobaloxime Macrocyclic Catalysts*

One of the most important families of precious metal-free catalysts are the cobaloximes, i.e. cobalt complexes with imine-OH moieties on macrocyclic ligands. There have been many examples of cobaloximes used with precious metal-based photosensitizers[4–6] but very few with organic photosensitizers. Richard Eisenberg and co-workers have published important work in this area, starting with the first completely precious metal-free TSC in 2009.[7] This system associated catalyst **1**, a cobalt complex with a macrocyclic ligand formed from two hydrogen-bonded dmg (dimethylglyoximate) units, with a TEOA (triethanolamine) SD and the commercial dyes **EY** and **RB** as the photosensitizers. This starting point for the development of precious metal-free systems afforded a $TON_{PS}$ (turn over number per mole of PS) and a $TON_{Cat}$ (turn over number per mole of catalyst) of 900 and 165 respectively when free $dmgH_2$ ligand was added into the system. The TONs were limited by the decomposition of both the photosensitzer and the catalyst. Although the presence of the heavy halogen atoms in the photosensitizer facilitates *isc* to the redox active triplet state, they also contribute to the decomposition of the dye via cleavage of the C-X bond. Consequently, in 2010 they employed halogen-free rhodamine photosensitizers substituted with heavy Group 16 atoms in the xanthene ring to facilitate *isc* and increase the TONs.[8] The TONs of 290 and 9000 for **1** and **Rhod-Se** respectively were for a long time the highest among the cobaloxime family when used with an organic photosensitizer.

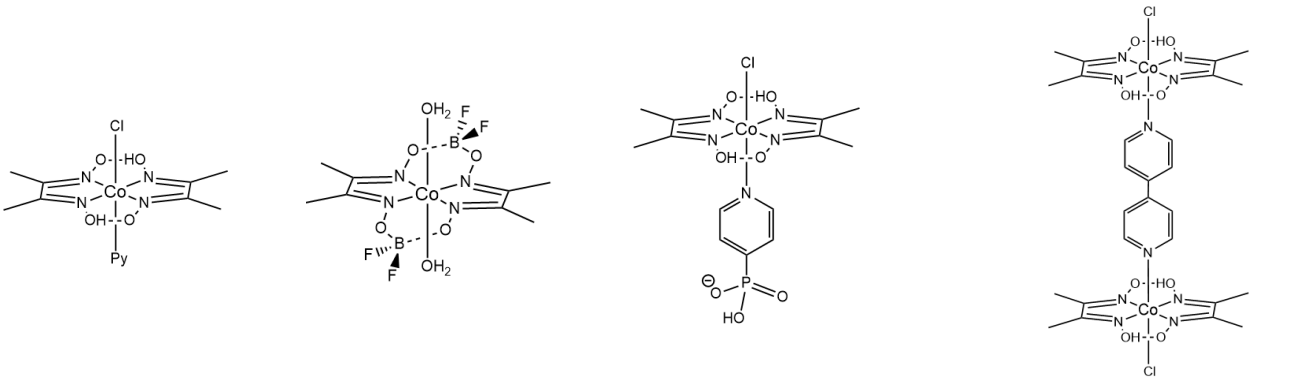

$Co(dmgH)_2pyCl$ **(1)** | $Co(dmgBF_2)_2(H_2O)_2$ **(2)** | $[Co(dmgH)_2Cl(Py\text{-}PO_3H)]^-$ **(3)** | $Co_2(dmgH)_4(\mu\text{-}4,4'\text{-}bpy)Cl_2$ **(4)**

***Figure 4:*** *Structures of cobaloxime catalysts used for proton reduction.*

The decomposition of **1** was later studied by Eisenberg by comparison of the activity of systems with separate catalyst and photosensitizer units to ones in which they were covalently linked.[9] They determined that the dmgH ligand decomposes during the catalytic cycle if the catalyst is unable to be reduced twice by the photosensitizer. However, they found that the reason for the increased longevity upon addition of free ligand can be attributed to ligand exchange during $H_2$ generation, meaning that the decomposed ligand can be replaced by a new one. Three factors were also identified as to why the connected Cat-PS system offered no advantage over the system in which they are separate. This was very good work as they carried out the necessary experiments to gain a detailed insight into how the catalytic system operates, a necessity for making future improvements on efficiency.

**1** was also used by J. Zhao and Z. Zhu in 2011 with **Acr** as the photosensitizer.[10] However, this system stopped producing $H_2$ after two hours and the TONs were lower than those reported by Eisenberg. Similarly poor activity was also reported by Y. Fan and co-workers in 2014 using binuclear catalyst **4** with **EY**.[11] It must be considered that the $TON_{Cat}$ for a binuclear catalyst cannot be fairly compared to a mononuclear catalyst as there are twice the number of cobalt centres able to produce $H_2$ per mole of catalyst.

***Table 1:*** *Collated data for TCS precious-metal free photocatalytic proton reduction.*

| Catalyst Family | Cat (conc.) | PS (conc.) | PS/Cat Ratio | SD (conc.) | Solvent | pH | Irradiation Source (λ) | $V_{H_2}$ / mL (hours) | $TON_{Cat}$ | $TON_{PS}$ | Quenching Pathway | Author (Year) [Ref] |
|---|---|---|---|---|---|---|---|---|---|---|---|---|
| Cobaloximes | **1** (248 μM) (+ 3 mM free ligand) | **EY** (50 μM) | 1/5 | TEOA (5%) | MeCN/$H_2O$ (1:1) | 7.0 | Xe (> 450 nm) | 20 (20 h) | 165 | 900 | Not mentioned | **R. Eisenberg (2009) [7]** |
| | **1** (300 μM) | **Rhod-Se** (19 μM) | 1/15.8 | TEOA (5%) | MeCN/$H_2O$ (1:1) | 7.0 | Luxeon Star Hex LED (520 nm) | 8.5 (8 h) | 290 | > 9000 | Reductive | **R. Eisenberg (2010) (8)** |
| | **1** (500 μM) | **Fl** (500 μM) | 1/1 | TEOA (5%) | MeCN/$H_2O$ (1:1) | 7.0 | Luxeon Star Hex LED (520 nm) | 3.6 (24 h) | 63 | 32 | Reductive | **R. Eisenberg (2011) (9)** |
| | **1** (250 μM) | **Acr** (150 μM) | 3/5 | TEOA (2.5%) | DMF/$H_2O$ (3:1) | 9.0 | Xe (> 420 nm) | 16.2 (2 h) | 132 | 110 | Reductive | **J. Zhao & Z. Zhu (2011) (10)** |
| | **2** (100 μM) | **RB** (400 μM) | 4/1 | TEA (10%) | MeCN/$H_2O$ (1:2) | 10.0 | Xe (> 400 nm) | 4 (5h) | 327 | 41 | Either | **L. Sun (2010) (12)** |
| | **3** (44 μM) | **EY** (22 μM) | 1/2 | TEOA (0.1 M) | $H_2O$ | 7.0 | Solar Light Simulator (> 420 nm) | 0.3 (1 h) | 73 | 63 | Not mentioned | **E. Reisner (2012) (13)** |
| | **4** (370 μM) | **EY** (400 μM) | 1.08/1 | TEOA (20%) | MeCN/$H_2O$ (1:1) | 10.0 | Xe (> 420 nm) | 36.4 (2 h) | 160 | 74 | Either | **Y. Fan (2014) (11)** |
| Iron Complexes & Hydrogenases | **5** (500 μM) | **EY** (500 μM) | 1/1 | TEA (10%) | $H_2O$ (+ Cyclodextrins) | 10.0 | Xe (> 450 nm) | 0.58 (24 h) | 190 | 95 | Oxidative | **L. Sun (2012) (17)** |
| | **6** ($4.44 \times 10^{-9}$ M) | **EY** (444 μM) | 100000/1 | TEOA (0.15 M) | $H_2O$ | 7.0 | Solar Light Simulator (> 420 nm) | 0.12 (24 h) | 500000 | 5 | Oxidative | **E. Reisner (2013) (19)** |
| | **7** (100 μM) | **EY** (200 μM) | 2/1 | TEA (10%) | $H_2O$ (+ SDS micelles) | 10.5 | Thorlabs LED (455 nm) | 0.86 (4.5) | 117 | 27 | Oxidative | **F. Gloaguen (2014) (18)** |
| | 8 (2 μM) | **Fl** (1.9 mM) | 950/1 | TEA (5%) | EtOH/$H_2O$ (1:1) | 12.5 | Green LED (520 nm) | 0.4 (24 h) | 2100 | 2 | Reductive | **W. McNamara (2016) (20)** |
| Cobalt/Nickel Complexes | **9** (140 μM) | **EY** (300 μM) | 2.14/1 | NaHA (100 mM) | MeCN/$H_2O$ (1:1) | 2.25 | Mercury Lamp (> 410 nm) | 1.1 (8 h) | 80 | 19 | Reductive | **R. Eisenberg & P. Holland (2011) (23)** |
| | **10** (4 μM) | **Fl** (20 mM) | 5000/1 | TEA (5%) | EtOH/$H_2O$ (1:1) | 12.2 | Green LED (520 nm) | 2.2 (40 h) | 5500 | 0.5 | Reductive | **R. Eisenberg & P. Holland (2012) (24)** |
| | **11** (4 μM) | **Fl** (20 mM) | 5000/1 | TEA (0.36 M) | EtOH/$H_2O$ (1:1) | 11.6 | Green LED (520 nm) | 3.8 (30 h) | 7335 | 0.8 | Reductive | **R. Eisenberg & P. Holland (2013) (25)** |
| | **12** (20 μM) | **Fl** (2 mM) | 100/1 | TEOA (0.35 M) | $H_2O$ | 9.8 | Green LED (520 nm) | 14.7 (> 100 h) | 6000 | 30 | Reductive | **R. Eisenberg & P. Holland (2015) (26)** |
| | **13** (200 μM) | **Fl** (2 mM) | 100/1 | TEA (5%) | MeCN/$H_2O$ (1:1) | 10.5 | Xe (> 400 nm) | 7.8 (12 h) | 320 | 16 | Oxidative | **C. Chen (2013) (28)** |
| | **14** (100 μM) | **Fl** (500 μM) | 5/1 | TEA (10%) | MeCN/$H_2O$ (1:3) | 10.0 | Xe (> 400 nm) | 0.17 (4 h) | 14 | 1.5 | Not mentioned | **C. Chen (2015) (29)** |
| | **15** (100 μM) | **EY** (400 μM) | 4/1 | TEA (10%) | MeCN/$H_2O$ 1:1) | 10.0 | Xe (> 420 nm) | 8.26 (4 h) | 676 | 85 | Either | **Y. Fan (2015) (30)** |
| | **16** (5 μM) | **Fl** (1 mM) | 200/1 | TEA (5%) | EtOH/$H_2O$ (1:1) | 12.3 | Xe (> 420 nm) | 4.67 (8 h) | 7634 | 19 | Reductive | **Y. Fan (2016) (27)** |
| | **17** (5 μM) | **Fl** (1 mM) | 200/1 | TEA (5%) | TEA (5%) | 12.0 | Green LED (520 nm) | 2.14 (24 h) | 3500 | 8.8 | Not mentioned | **N. Verani (2016) (31)** |

* Information not included and therefore calculated in this work

In 2010 L. Sun and co-workers modified **1** to improve the $TON_{Cat}$ using catalyst **2** with **RB** and TEA (triethylamine).[12] Replacing the H bridges with $BF_2$ bridges increased the stability of the catalyst as the stronger O-B interaction helps to keep the ligands coordinated to the cobalt. These ligands also increase the reduction potential of the complex therefore making electron transfer from the photosensitizer more favourable. A $TON_{Cat}$ of 327 was achieved after 5 hours of irradiation. Whilst this is greater than the TON reported by Eisenberg, the longevity of the system is much shorter. They also investigated the effect of pH on the system. The optimum pH was found to be 10; at higher pH the concentration of protons was too small to protonate the reduced Co(I) species to form the hydride needed to form $H_2$, and at lower pH the rate of formation of the Co(I) species was too low.

Most publications in this field report the use of mixed aqueous/organic solvents under anaerobic conditions. Anaerobic conditions are used to prevent quenching of the excited triplet state of the photosensitzer by $O_2$ ($O_2$ exists as a triplet in the ground state). However, given that the ultimate aim is to produce $H_2$ on an industrial scale via water-splitting, these conditions would not be suited for the application. In 2012, Erwin Reisner reported an analogue of Eisenberg's first system (**1**, **EY**, TEOA) that worked in an aqueous medium in the presence of oxygen.[13] Catalyst **3** was prepared by implementing a phosphonic acid group on the pyridine ligand of **1**, therefore enabling solubility in water. In the presence of $O_2$ there was only a 30% loss in activity, however the TONs for this system are still relatively low. Furthermore, no explanation as to why there is only slow quenching of the photosensitizer in this system compared to others is offered.

## *V) Iron Complexes and Hydrogenases*

Being a highly abundant metal, iron is a good metal of choice for photocatalytic complexes. In nature, iron is used by microbes in the active sites of hydrogenase enzymes for the reduction of protons. Given that nature has evolved to carry out chemical processes in a much more efficient manner than our methods, there have been countless efforts to develop bio-mimetic systems for photocatalytic $H_2$ production.[14–16] Hydrogenase active sites are either mononuclear iron complexes or binuclear Fe-Fe or Ni-Fe centres with bridging cysteine units. Bio-mimics are therefore similar iron complexes with bridging thiolate ligands. However, these bio-mimics suffer from poor solubility in water, poor stability and low tolerance to $O_2$. In contrast to the cobaloximes, the catalytic cycles with these complexes tend to take the oxidative quenching pathway.

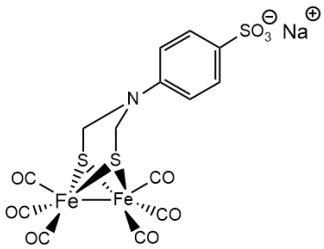


**(5)**

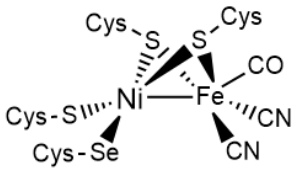


[NiFeSe] active site of *Db* hydrogenase

**(6)**

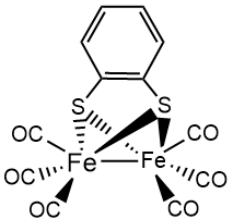


$Fe_2(\mu\text{-bdt})(CO)_6$

**(7)**

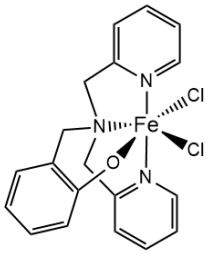


**(8)**

***Figure 5:*** *Structures of bio-mimetic hydrogenase and iron catalysts used for proton reduction.*

There have been few demonstrations of these complexes as catalysts with organic dyes. The first was by Sun and co-workers in 2012.[17] To overcome the problem of solubility they prepared host-guest structures of catalyst **5** contained within the cavities of cyclodextrins (CDs). CDs are supramolecular sugar units with hydrophilic exteriors that enable water solubility, and hydrophobic interiors capable of solubilising hydrophobic substrates. It was found that incorporating both **5** and **EY** into the cavities increased their photostabilities and thus afforded greater TONs compared to the free compounds in aqueous solution. They attribute the increased stability of **5** to the likeliness of the CD environment to that of the protein-protective environment of a hydrogenase active site. Despite the low TONs of this system, the use of CDs has potential as they are easily and cheaply made.

A similar approach to overcoming solubility was employed by F. Gloaguen and co-workers in 2014 where they incorporated catalyst **7** and **EY** into sodium dodecyl sulfate (SDS) micelles.[18] However, both the TONs and the longevity of the system were lower than those of the **5/EY** system. Interestingly, the TON for the **7/EY** system under similar conditions was higher in the absence of SDS micelles than the TON for the **5/EY** system in the absence of CDs. This suggests that perhaps catalyst **7** is more effective than catalyst **5**, but the effect of CDs is greater than the effect of SDS micelles.

In 2013, Reisner reported a $TON_{Cat}$ of 500000 using a [NiFeSe]-hydrogenase enzyme from *Desulfomicrobium baculatum.*[19] Whilst this system worked under favourable conditions (pH 7.0, fully aqueous solvent), the seemingly impressive $TON_{Cat}$ cannot be considered a triumph as the concentration of the hydrogenase was 4.4 nM. At such low concentrations, it is no surprise that each $H_2$-evolving site turns over so many moles of $H_2$. Catalyst concentration should always be considered when comparing TONs of these systems because lower concentrations will always increase $TON_{Cat}$, but the amount of $H_2$ evolved will be extremely small. It was also reported that the system still functioned under 'high' levels of $O_2$, however at the atmospheric concentration of 21% $O_2$ only 10% of the anaerobic activity remained.

A recent example of very efficient $H_2$ production was demonstrated by W. McNamara and co-workers in 2016.[20] This mononuclear iron polypyridine complex (**8)** was capable of TONs of over 2100 when used with **Fl**. They used a high PS/Cat ratio which is known to increase $TON_{Cat}$ as electron transfer to the catalyst is more likely when each catalyst complex is surrounded by several photosensitizer molecules.

## *VI) Nickel and Cobalt Complexes*

More recently, efficient precious metal-free systems have been demonstrated with nickel or cobalt catalysts with pyridinethiolate or phosphorus ligands. These catalysts are used owing to their success or the success of similar complexes in electrocatalytic reduction of protons as several examples of efficient systems have recently been reported, for example by DuBois and co-workers.[21,22]

Eisenberg and Patrick Holland have made some significant contributions in this field. Their first was in 2011 where they used catalyst **9**, a complex based on one previously used by DuBois, with **EY**, but the $TON_{Cat}$ of 80 was poor.[23] Interestingly, this is the only example of a precious metal-free system operating in acidic conditions (pH 2.25), and as such the SD was sodium ascorbate (NaHA). Between 2012 and 2015 Eisenberg and Holland reported efficient proton reduction using **Fl** with nickel pyridinethiolate catalysts **10**, **11** and **12** to achieve TONs of 5500, 7335 and 6000 respectively.[24–26] Such high TONs arose due to the use of high PS/Cat ratios (large excess of PS makes reduction of the catalyst more favourable) and very good stability of the catalyst, leading to systems with longevities of up to 100 hours.

In 2016, Fan reported, to the best of our knowledge, the most efficient proton reduction system without precious metals. Catalyst **16**, closely resembling **11**, was used under similar conditions to yield a $TON_{Cat}$ of 7634.[27] The **11/EY** and **16/EY** system produced roughly the same amount of $H_2$, yet the longevity of the **11/EY** system was greater (30h *vs.* 8h). This can likely be attributed to the significantly greater concentration of **Fl** used in the **11/EY** system, suggesting that **16** is the more efficient catalyst but was more limited by **Fl** decomposition. Whilst the **11/EY** and **16/Fl** systems may afford the highest TONs, use of **12/Fl** is more favourable as it works in purely aqueous conditions.

Other reports of proton reduction from catalysts of the same family include the **13/Fl** and **14/Fl** from C. Chen in 2013 and 2015.[28,29] However the TONs of 320 and 14 are relatively low and do not compete with those discussed earlier, and system longevity was short. Similarly, Fan reported a $TON_{Cat}$ of 676 for catalyst **15** with

**EY** in 2015.[30] Finally, N. Verani reported catalyst **17** with **Fl** in 2016 with a TON of 3500.[31] This is a big improvement on the similar complex **14**. Although the PS/Cat ratio is better optimised, the system longevity was much greater.

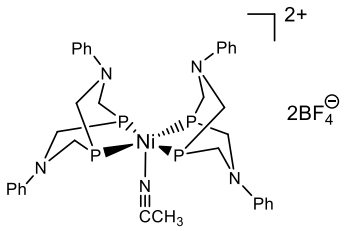

$[Ni(P_2^{Ph}N_2^{Ph})_2](BF_4)_2$

**(9)**

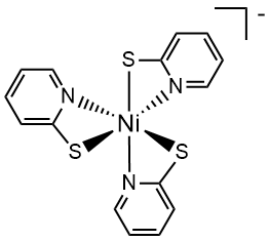

$[Ni(pyS)_3]^-$

**(10)**

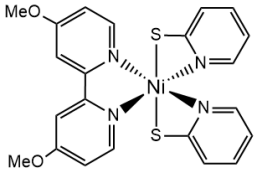

$Ni(4,4'\text{-}OMe\text{-}2,2'\text{-}bpy)(pyS)_2$

**(11)**

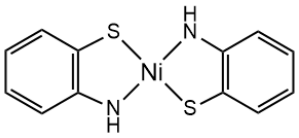

$Ni(abt)_2$

**(12)**

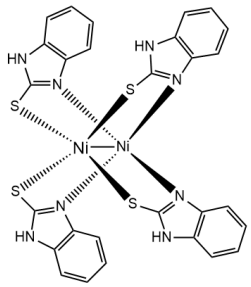

$Ni_2(MBD)_4$

**(13)**

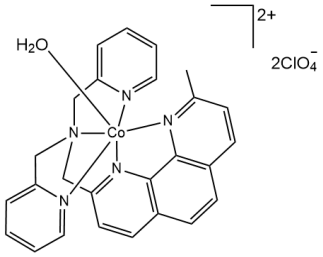

$[Co(Dmphen\text{-}DPA)(H_2O)](ClO_4)_2$

**(14)**

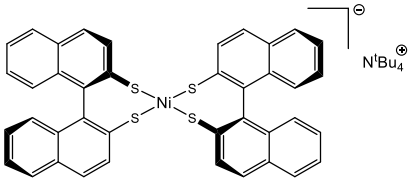

$[Ni(BNT)_2]N^tBu_4$

**(15)**

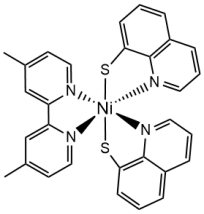

$Ni(Hqt)_2(4,4'\text{-}CH_3\text{-}2,2'\text{-}bpy)$

**(16)**

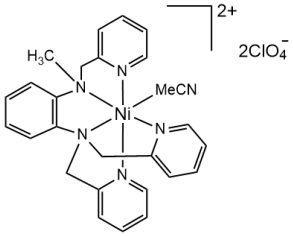

$[Ni(L^{N2Py3})(MeCN)](ClO_4)_2$

**(17)**

***Figure 6:*** *Structures of cobalt/nickel pyridinethiolate catalysts used for proton reduction.*

## *VII) Conclusion and Future Directions*

The photocatalytic reduction of protons using precious metal-free TCSs is an attractive way of generating $H_2$. Whilst there is a plethora of catalysts available for electrocatalytic and/or photocatalytic proton reduction, there are few examples utilising organic dyes as photosensitizers. This review has given an insight into three important families of catalysts that have been tested with organic photosensitizers: cobaloximes, hydrogenases and cobalt/nickel pyridinethiolate complexes. Most these systems proceed via a reductive quenching pathway despite often have higher rate constants for oxidative quenching. This is most likely due to the extremely high concentration of SD compared to the catalyst.

Future research must focus on the development of efficient and stable organic photosensitizers if these systems are to compete with systems involving precious metals. As seen in this report, there are only a handful of organic photosensitizers currently available. Whilst organic photosensitizers other than those mentioned in this report

exist, there are few examples and their activities are poor. Most systems are limited by the poor stability of the photosensitizers; it is known that the radical anions of these compounds which are formed during the reductive quenching pathway is unstable. Research should also focus on developing systems with more realistic operating conditions, i.e. pH 7.0, no organic solvents, and presence of $O_2$. A balance between $TON_{Cat}$ and the moles of $H_2$ produced needs to found because high TONs are useless if the system produces very little $H_2$. Comparison of systems can be very difficult as they are sensitive to many factors. For example, can we compare systems which used a fixed wavelength irradiation source against ones which use a range of wavelengths? Perhaps the future should see standardization of such conditions. Finally, future research should also aim to develop systems which can simultaneously generate $H_2$ and $O_2$ so that the ultimate aim of developing a water-splitting device can be achieved.

# Project Report: The Synthesis and Study of Precious Metal-Free Three-Component Photocatalytic Systems for the Reduction of Protons to $H_2$

## I) Abstract

*The use of a triazatriangulenium organic dye known as **TATA**$^+$ as a photosensitizer in a completely precious metal-free photocatalytic system for the reduction of protons to $H_2$ was investigated. When used in association with the cobalt catalyst $[Co(CR)(H_2O)_2]^{3+}$ (10 μM) and ascorbate (0.1 M) as a sacrificial electron donor, the system can achieve turn-over-numbers greater than 4000 upon visible light irradiation (400-700 nm) at pH 4.5 with a photosensitizer concentration of 250 μM. In terms of stability and activity, **TATA**$^+$ exceedingly outperforms any organic photosensitizer and the complex $[Ru(bpy)_3]^{2+}$ which is often used as a benchmark. Where other recently reported organic photosensitizers rapidly decompose from their reduced state in acidic conditions, **TATA**$^+$ is stable in its reduced radical state and shows little decomposition after 46 hours of irradiation. The excellent stability of the reduced state can be attributed to the delocalisation of the radical across the planar structure and stabilization from three electron-donating nitrogen atoms.*

*The synthesis of cobalt and iron complexes containing polypyridine-(bis)imine ligands as potential proton reduction catalysts was also attempted. The complexes were formed in their +2 oxidation state and showed reduction processes, as required for catalysis, in the cyclic voltammograms. $[Co(LPI)(MeCN)_2](BF_4)_2$ (LPI = phenanthroline-(bis)imine ligand) displayed a reversible reduction potential of -1.45 V vs SCE for the $E(Co^{II}/Co^{I})$ redox couple suggesting that it may be active towards proton reduction if used in conjunction with $[Ru(bpy)_3]^{2+}$. $[Fe(LPI)Cl_2]$ displayed a reversible reduction potential of -0.94 V vs SCE for the $E(Fe^{II}/Fe^{I})$ redox couple which suggests that it could be used in conjugation with **TATA**$^+$. Two other iron complexes were reported, $[Fe(LPI)(EtOH)_2](BF_4)_2$ and $[Fe(LBI)(EtOH)_2](BF_4)_2$ (LBI = bipyridine-(bis)imine ligand), however the process for the $E(Fe^{II}/Fe^{I})$ redox couples were irreversible.*

## II) Introduction

How can we meet the expected increase in the global energy demand in a clean and renewable fashion? This is currently one of the most important questions being asked of science following a century of intense fossil fuel combustion which has led to catastrophic environmental consequences. Solar power is unquestionably the most abundant renewable energy source and hence there is a drive to develop viable systems for harvesting solar radiation. This requires solar photons to be captured, their energy stored, transported and then utilized on demand. One method of doing this is to store the energy in the chemical bonds of molecules, or 'energy carriers'. Perhaps the biggest contender for such an energy carrier is molecular hydrogen, $H_2$. Hydrogen has the advantage of being 3x more energy dense than petroleum and the only product of its combustion is water.[1] To retrieve the energy in $H_2$ bonds (+286 kJ mol$^{-1}$) hydrogen could be used in fuels cells or directly in internal combustion engines.

An attractive way of forming $H_2$ using solar power is via water-splitting, i.e. the oxidation of $H_2O$ into $2H^+$ and $½O_2$ followed by proton reduction to $H_2$. Much research has been carried out over the past few decades into developing molecular photocatalytic systems for the reductive half-equation to form $H_2$.[32–34] Such systems normally comprise three components and are hence called three-component systems (TCSs). These include a photosensitizer (PS) to harvest the light, a redox catalyst and a sacrificial electron donor (SD). The photosensitizer is a light-harvesting molecule/complex which captures photons to promote an electron to a higher energy level. Ultimately, the energy of the photon is manifested into an electron transfer from the SD to the catalyst via the photosensitizer. The order of the electron transfer processes depends on which quenching pathway is taken (Fig. 1). The catalyst in the reduced state is able to generate $H_2$, the mechanism of which varies

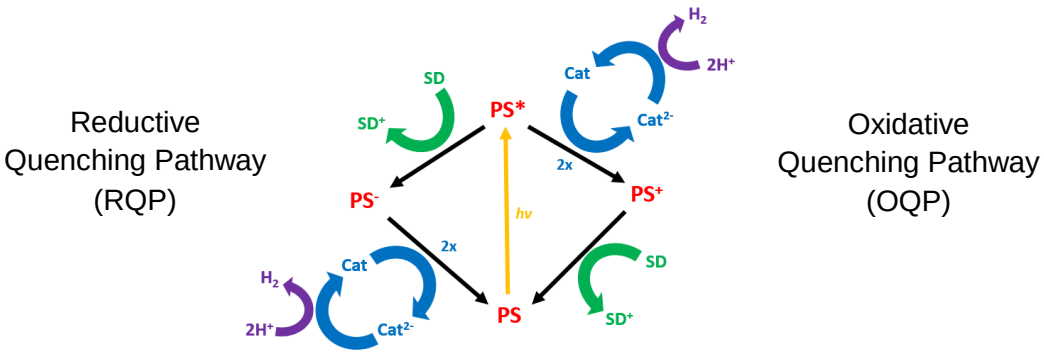


***Figure 1:*** *The general mechanism for $H_2$ production in in a TCS via oxidative or reductive quenching of the photosensitizer.*

depending on the nature of the system but usually involves protonation of the reduced catalyst species to form a hydride as the first step. TCSs can be judged by several factors such as system longevity and durability, moles/volume of $H_2$ generated or the rate of $H_2$ production. The rate of $H_2$ production is known as the turn-over frequency (TOF) and the initial TOF indicates the inherent photocatalytic activity of the system. However the principle consideration is the turn-over number (TON) per catalyst (i.e. the number of catalytic cycles that one molecule/complex can undergo) as this gives information about the overall stability of the system.

The SD is used to provide a source of electrons for proton reduction. This occurs indirectly, whether it be to PS* in the RQP or to $PS^+$ in the OQP. The choice of SD depends on the conditions of the system and the choice of PS. The high concentration of SD used in TCSs results in the RQP usually being taken as PS* comes into contact with many more SDs than catalyst complexes.[35]

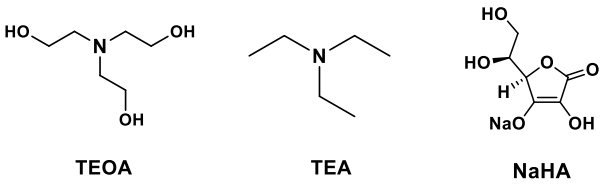


***Figure 2:*** *Common sacrificial electron donors used in TCSs for proton reduction.*

Whilst reasonably efficient TCSs containing precious metals exist (either as part of the catalyst or the photosensitizer)[36–43], there is an obvious need to develop systems that use cheaper and more abundant metals. This project is divided into two sections: the investigation of a precious metal-free TCS using a novel organic photosensitizer, and the synthesis of new precious metal-free complexes as potential $H_2$-evolving catalysts.

The first aspect of the project is concerned with the investigation of the use of an organic dye as a photosensitizer. Currently, the most efficient photosensitizers are complexes based around ruthenium[44–48], rhenium[37,49] or iridium[50,51]. The prototypical photosensitizer used is tris(bipyridine)ruthenium(II) chloride, $[Ru(bpy)_3]Cl_2$ (denoted **Ru)**. For the application as a photosensitizer, this complex offers suitable photochemical and redox properties, good solubility in water and strong absorption in the visible region (14,600 $M^{-1}$ $cm^{-1}$ at 450 nm).[3] Organic dyes can serve as ideal replacements to these transition metal complexes which are expensive environmental burdens. There are currently few classes of organic photosensitizers used for proton reduction, and even fewer have been efficiently used in association with a precious metal-free catalyst. In such systems, organic dyes have not been able to match the photosensitizing abilites of complexes like **Ru**. Commercial dyes based around the xanthene moiety such as Fluorescein (**Fl**)[24–27,31], Eosin Y (**EY**)[11,17] and Rose Bengal (**RB**)[12] have had the most success. As summarized in the literature review, Richard Eisenberg and Yao-Ting Fan have demonstrated efficient systems using nickel pyridinethiolate complexes with **Fl** achieving TONs in the range of 5000-8000 (*vs* catalyst), however these systems have all used very high PS/Cat ratios with high concentrations of photosensitizer (> 1

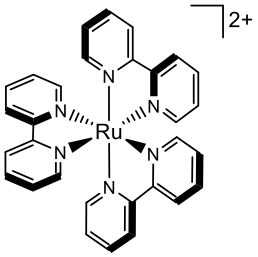


***Figure 3:*** *$[Ru(bpy)_3]^{2+}$(**Ru**).*

mM).[24–27] Other classes of organic photosensitizer include rhodamines[8], acriflavines[10], bodipys (boron-dipyrromethene)[52–54] and perylenes[53,55]. None of these dyes have produced significant amounts of $H_2$ when used with a precious metal-free catalyst (typically less than 1 mL) and system longevities are short. Moreover, most of these systems can only function in a basic aqueous/organic media due to poor solubility and stability in water. However, given that the ultimate aim is to produce $H_2$ via water-splitting, it is of the utmost importance to develop photocatalytic systems that will operate efficiently in water. As such, there is clearly a need for the development of new efficient organic photosensitizers which are stable over a long period in a purely aqueous media.

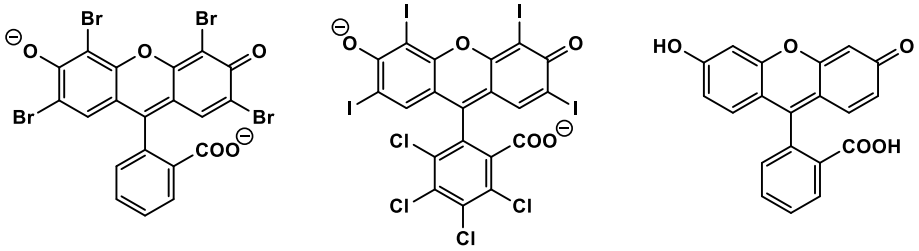


Eosin Y **(EY)** | Rose Bengal **(RB)** | Fluorescein **(Fl)**

***Figure 4:*** *Structures of the most common commercial organic photosensitizers.*

This project reports the use of a novel organic dye as a photosensitizer for proton reduction in a purely aqueous media. The dye is a triazatriangulenium cation known as [TATA-(EE)$_3$]Cl (denoted **TATA$^+$**) and was synthesised by a team in the Laboratoire ITODYS at the Université Paris. Its cationic charge enables excellent water solubility which is not something that other organic photosensitizers can boast. It has a molar absorption coefficient of 8800 $M^{-1}$ $cm^{-1}$ (532 nm) and a reduction potential of -1.18 V (*vs* SCE). This potential is lower than most organic photosensitizers and is sufficicently negative enough to achieve reduction of the $H_2$-evolving catalyst.

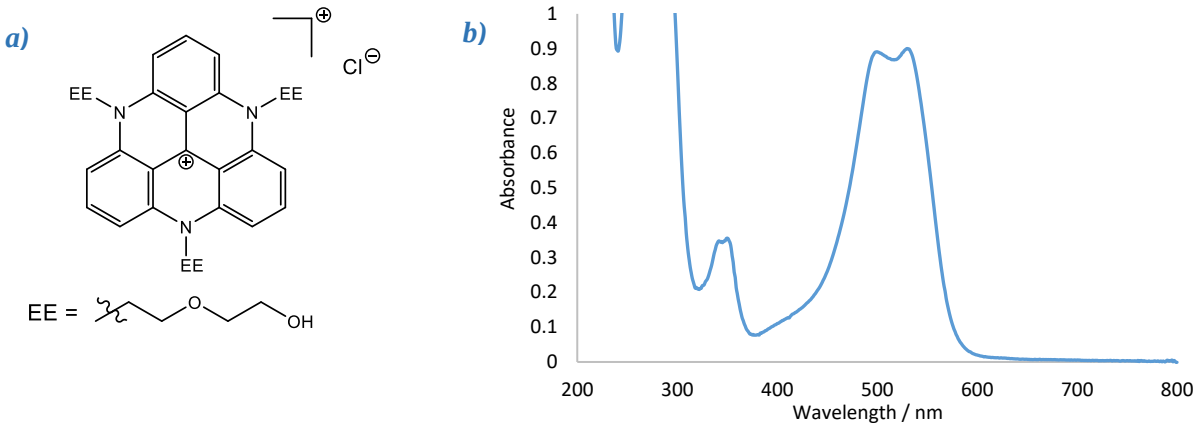


***Figure 5:*** *a) Structure of **TATA$^+$**; b) UV-Vis spectrum of **TATA$^+$** in $H_2O$ at 1 mM (l = 1 mm).*

Preliminary work by CIRE has demonstrated that **TATA$^+$** is a very efficient photosensitizer for proton reduction in water using the cobalt catalyst $[Co^{III}(CR)(H_2O)_2]^{3+}$ (CR = 2,12-dimethyl-3,7,11,17-tetra-azabicyclo(11.3.1)-heptadeca-1(17),2,11,13,15-pentaene) and ascorbate ($HA^-$) as the SD. This system is capable of achieving TONs greater than 1000 at photosensitizer concentrations as low as 100 µM and catalyst concentration of 10 µM for up to 22h. The aim of this project was to further investigate and optimise this system by carrying out photocatalysis experiments and varying the conditions to observe the effect.

The catalyst, known as **14PDN**, is a macrocyclic pyridine-(bis)imine cobalt complex which was developed by CIRE and is very stable and active towards proton reduction.[45,56] It can achieve TONs of up to 1000 at a concentration of 100 μM in association with **Ru**. Whilst much higher TONs have been reported, this was the highest TON for a catalyst at such a high concentration. The stability of this complex can be attributed to the stabilizing delocalisation of electrons on the $Co^{I}$ species formed during the catalytic cycle. The $Co^{I}$ species is in fact in equilibrium between $[Co^{I}(CR)(H_2O)]^{+}$ and $[Co^{II}(CR^{\bullet-})(H_2O)_2]^{+}$ in which the radical is delocalised across the pyridine-imine moiety. It has been demonstrated that the active catalyst species is $[Co^{II}(CR)(H_2O)_2]^{2+}$ which is formed via reduction by ascorbate.[45,56]

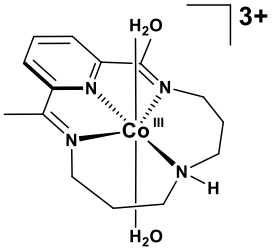


***Figure 6:*** *$[Co^{III}(CR)(H_2O)_2]^{3+}$ (**14PDN**).*

The second section of the project is devoted to the development of new precious metal-free complexes as potential $H_2$-evolving catalysts for proton reduction. There is a wide range of complexes used to reduce protons electrochemically and/or photochemically.[32,34,57–59] The most efficient are usually limited to rhodium[40,43,44] and platinum[41] complexes but efficient cobalt[7,10,38,45,56,60–64], nickel[65] and iron-hydrogenase[57] complexes have also been reported. A good $H_2$-evolving catalyst should be photochemically inert, possess suitable redox potentials, be able to bind protons to produce $H_2$ by proton-electron transfers, soluble and stable in water, and cheap.

Reported in this work is the synthesis of potential catalysts with tetraaza polypyridine-(bis)imine (polypyridine = bipyridine or phenanthroline) ligands based on first-row transition metals. The polypyridine-(bis)imine moiety is being explored as it should provide even more stabilisation to the $Co^{I}$ species through increased electron delocalisation, compared to **14PDN**. However, direct analogues of **14PDN** with bipyridine or phenanthroline in replacement of pyridine would present too much strain from being pentadentate in the same plane. In fact, the synthesis of such complexes was attempted for this project but was unsuccessful. As such, the synthesis of complexes incorporating open polypyridine-(bis)imine ligands was attempted (Fig. 7). The bulky $^{i}Pr$ groups should provide steric hindrance against two ligands coordinating to the metal. Whilst complexes of Co, Ni and Fe with similar (bis)imine ligands have been synthesised before[66,67], only the structural characterization has been made and no electrochemical or photocatalytic studies have been carried out. All the specific complexes presented in this report are new complexes.

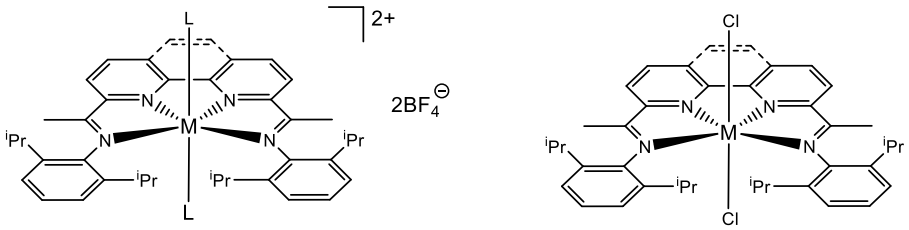


***Figure 7:*** *General structures of the target complexes. L = solvent (MeCN or EtOH). M = Co or Fe.*

It should be noted that these complexes can be considered analogous to tetraaza polypyridine complexes that have been reported (Fig. 8). In 2012, T. Lau reported that $[Co(qpy)(OH_2)_2]^{2+}$ (qpy = 2,2′:6′,2″:6″,2‴-quaterpyridine) can efficiently catalyse the oxidation and reduction of water to $O_2$ and $H_2$ respectively in association with ruthenium and iridium photosensitizers upon visible light irradiation.[64] In 2016, T. Lau and M. Robert also demonstrated that the same catalyst and its iron analogue can photocatalytically reduce $CO_2$ to more useful molecules such as CO and methanol when used with an organic dye (purpurin) or **Ru**.[46]

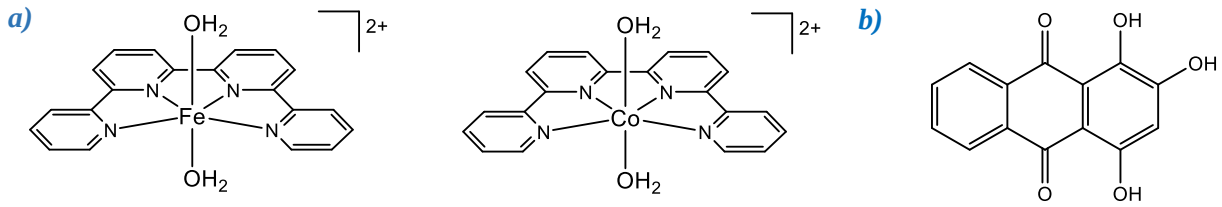


***Figure 8:*** *a) Quaterpyridine catalysts reported by T. Lau and M. Robert; b) Structure of the organic photosensitizer purpurin.*

## *III) Experimental Procedures*

**2,9-Diacetyl-1,10-phenanthroline (L1)**
A mixture of 2,9-dichloro-1,10-phenanthroline (0.5 g, 2.0 mmol), tributyl(1-ethoxyvinyl)tin (1.5 g, 4.15 mmol, 2.075 equivalents) and $Pd(PPh_3)_2Cl_2$ (0.125 g, 0.18 mmol, 0.09 equivalents) were stirred in freshly distilled DMF (5 mL) at 80°C for 60 hours under an inert argon atmosphere. The resulting brown suspension was cooled and poured into a KF solution (3.5 g in 25 mL $H_2O$) to give a brown precipitate. The precipitate was washed with $Et_2O$ to extract the product and $CH_2Cl_2$ (~ 40 mL) was added to the ether extract. The mixture was washed with water (3 x 30 mL), dried over $Na_2SO_4$ and the solvent removed to give a brown solid. Purification on an alumina column using a cyclohexane-$Et_2O$ eluent (10:1 to 5:1) yielded 2,9-di(1-ethoxyvinyl)-1,10-phenanthroline as a white solid (391 mg, 61.6 %). $^1$H NMR ($CDCl_3$, 400 MHz, Fig. S2): $\delta$ 8.22 (d, 2H, $J$ = 8.4 Hz, ArH), 8.07 (d, 2H, $J$ = 8.4 Hz, ArH), 7.73 (s, 2H, ArH), 6.05 (s, 2H, $=CH_2$), 4.58 (s, 2H, $=CH_2$), 4.09 (q, 4H, $J$ = 7.2, 6.8 Hz, $CH_2$), 1.51 (t, 6H, $J$ = 6.8 Hz, $CH_3$).
HCl (3.5 mL, 2 M) was added to 2,9-di(1-ethoxyvinyl)-1,10-phenanthroline (200 mg) and stirred in acetone at room temperature for 22 hours. The solvent was removed and $CH_2Cl_2$ (5 mL) and water (5 mL) were added. The organic layer was collected, washed with aqueous $NaHCO_3$ (10 mL) and water (2 x 10 mL), and then dried over $Na_2SO_4$. The solvent was removed to give a colourless crude product which was purified on an alumina column using $CH_2Cl_2$ to yield **L1** as a white solid (137 mg, 82.7 %). $^1$H NMR ($CDCl_3$, 400 MHz, Fig. S3): $\delta$ 8.43 (s, 4H, ArH), 7.97 (s, 2H, ArH), 3.10 (s, 6H, $CH_3$).

**6,6'-Diacetyl-2,2'-bipyridine (L2)**
The reaction was carried out under an inert argon atmosphere and temperatures maintained using a cryostat in a pentane bath. THF, $Et_2O$ and N,N-dimethylacetamide were freshly distilled prior to the synthesis. The exact concentration of $^n$BuLi in the bottle was determined via titration against benzyl alcohol in toluene with a phenanthroline indicator.
$^n$BuLi (3.05 mL of a 2.3 M solution in hexane, 7.01 mmol, 2.2 equivalents) was added to a stirring solution of THF (32 mL) at -80°C. 6,6'-Dibromo-2,2'-bipyridine (1 g, 3.18 mmol) was dissolved in 57 mL THF and then added dropwise to the $^n$BuLi solution to give a dark red solution and left to stir for 2h. A solution of N,N-dimethylacetamide (0.71 mL, 7.63 mmol, 2.4 equivalents) in $Et_2O$ (16 mL) was then added dropwise to the solution over 20 mins and then left to stir for 90 mins. The mixture was then heated to -15°C and HCl (6.36 mL at 6 M) added to afford a dark red residue which was isolated by rotary evaporation. The residue was cooled in an ice bath and NaOH (aq, 20% w/w) was added until pH ~10 was reached. The solid was filtered, air-dried and then recrystallized in ethanol to give off-white crystals of **L2** (0.2236 g, 29.3 %). $^1$H NMR ($CDCl_3$, 400 MHz, Fig. S4): $\delta$ 8.74 (dd, 2H, $J$ = 7.6, 1.2 Hz, ArH), 8.11 (dd, 2H, $J$ = 8.0, 1.2 Hz, ArH), 8.01 (t, 2H, $J$ = 8.0 Hz, ArH), 2.85 (s, 6H, $CH_3$).

**2,9-bis(ketimino)-1,10-phenanthroline(2,6-diisopropylaniline) (LPI)**
2,9-Diacetyl-1,10-phenanthroline (324 mg, 1.23 mmols) was dissolved in 2,6-diisopropylaniline (2.3 mL, 10 equivalents) at 160°C for 15 mins in a well purged flask under an argon atmosphere. A catalytic amount of formic acid (2 µL) was added to the dark brown solution which was then stirred at 180°C for 20 mins. The excess amine was removed by reduced pressure distillation to give a brown paste that afforded a yellow precipitate upon addition of ethanol. The precipitate was filtered and washed in ethanol (3 x 2 mL) to give **LPI** as a yellow solid (557 mg, 77.7 %). $^1$H NMR ($CDCl_3$, 300 MHz, Fig. S5): $\delta$ 8.84 (d, 2H, $J$ = 8.4 Hz,), 8.40 (d, 2H, $J$ = 8.7 Hz, ArH), 7.96 (s, 2H, ArH), 7.19 (d, 4H, $J$ = 6.6 Hz, ArH), 7.11 (t, 2H, $J$ = 6.3 Hz, ArH), 2.83

(m, 4H, $CHMe_2$), 2.57 (s, 6H, $CH_3$), 1.17 (d, 24H, $J$ = 6.9 Hz, $CH_3$). ESI (Fig. S6): *m/z* 583.5 $[M + H]^+$, 605.5 $[M + Na]^+$, 621.5 $[M + K]^+$. IR (KBr, Fig. S7): 3441, 3067, 2960, 2865, 1638, 1586, 1545, 1498, 1462, 1431, 1365, 1311, 1190, 1124, 1101, 872, 771, 755 $cm^{-1}$.

**6,6'-bis(ketimino)-2,2'-bipyridine(2,6-diisopropylaniline) (LBI)**
6,6'-diacetyl-2,2'-bipyridine (244.7 mg, 1.018 mmols) was dissolved in 2,6-diisopropylaniline (1.92 mL, 10 equivalents) at 160°C for 15 mins in a well purged flask under an argon atmosphere. A catalytic amount of formic acid (2 µL) was added to the dark brown solution which was then stirred at 180°C for 20 mins. The excess amine was removed by reduced pressure distillation to give a brown paste that afforded a pale lemon-coloured precipitate upon addition of ethanol. The precipitate was filtered and washed in ethanol (3 x 2 mL) to give **LBI** as a lemon coloured solid (438 mg, 77.0 %). $^1H$ NMR ($CDCl_3$, 400 MHz, Fig. S8): $\delta$ 8.65 (d, 2H, $J$ = 6.8 Hz, ArH), 8.41 (d, 2H, $J$ = 6.8 Hz, ArH), 7.96 (t, 2H, $J$ = 7.6 Hz, ArH), 7.19 (d, 4H, $J$ = 6.8 Hz, ArH), 7.12 (t, 2H, $J$ = 6.4 Hz, ArH), 2.80 (m, 4H, $CHMe_2$), 2.35 (s, 6H, $CH_3$), 1.17 (dd, 24H, $J$ = 6.8, 2.4 Hz, $CH_3$). ESI (Fig. S9): *m/z* 559.5 $[M + H]^+$, 581.5 $[M + Na]^+$. IR (KBr, Fig. S10): 3437, 3071, 2960, 2926, 2865, 1636, 1571, 1438, 1382, 1362, 1301, 1242, 1191, 1117, 1077, 990, 813, 777, 745 $cm^{-1}$.

**$[Co(LPI)(CH_3CN)_2](BF_4)_2$ (CoLPI)**
**LPI** (100 mg, 0.172 mmols) and $Co(BF_4)_2.6H_2O$ (1.1 equivalents, 0.189 mmol, 64.4 mg) were stirred in acetonitrile (20 mL) at 70°C for 4 hours. The resulting orange solution was cooled to room temperature and addition of $Et_2O$ yielded **CoPLI** as a deep-yellow precipitate (138 mg, 94.5 %). The precipitate was recrystallized by the slow vapour diffusion of diisopropyl ether into acetonitrile to yield orange crystals. IR(KBr, Fig. S11): 3428, 2971, 2870, 2309, 2281, 1638, 1622, 1507, 1466, 1443, 1386, 1369, 1300, 1187, 1084, 1003, 870, 792, 758 $cm^{-1}$. ESI (Fig. S12): *m/z* 302.7 $[Co(LPI)]^{2+}$, 768.2 $[Co(LPI)(MeCN)]BF_4$.

**$[Fe(LPI)(OH_2)_2](BF_4)_2$ (FeLPI)**
The synthesis and the subsequent work-up were performed in a glovebox. **LPI** (100 mg, 0.172 mmols) and $Fe(BF_4)_2.6H_2O$ (1 equivalent, 57.9 mg) were stirred in refluxing ethanol (20 mL) at 100°C overnight. The resulting dark purple solution was cooled to room temperature and a purple precipitate was obtained. The precipitate was vacuum filtered and washed with diethyl ether (2 x 10 mL) to yield **FeLPI** (48.5 mg, 32.2 %). IR (KBr, Fig. S13): 3406, 1671, 1619, 1605, 1509, 1460, 1421, 1392, 1365, 1294, 1273, 1261, 1210, 1149, 1084, 869, 768, 749 $cm^{-1}$.

**$[Fe(LBI)(OH_2)_2](BF_4)_2$ (FeLBI)**
The synthesis and the subsequent work-up were performed in a glovebox. **LBI** (86 mg, 0.15 mmols) and $Fe(BF_4)_2.6H_2O$ (1 equivalent, 51.9 mg) were stirred in refluxing ethanol (20 mL) at 100°C overnight. The resulting dark purple solution was cooled to room temperature and a purple precipitate was obtained. The precipitate was vacuum filtered and washed with diethyl ether (2 x 10 mL) to yield **FeLBI** (40.6 mg, 32.8 %). IR (KBr, Fig. S14): 3397, 3092, 1685, 1675, 1595, 1484, 1437, 1364, 1325, 1252, 1202, 1188, 1141, 1062, 1021, 809, 642, 613 $cm^{-1}$.

**$Fe(LPI)Cl_2$**
The synthesis and the subsequent work-up were performed in a glovebox. **LPI** (100 mg, 0.172 mmols) and $FeCl_2$ (1 equivalent, 21.2 mg) were stirred in refluxing butan-1-ol (10 mL) at 100°C overnight. The resulting green solution was cooled to room temperature and a green precipitate was obtained. The precipitate was vacuum filtered and washed with diethyl ether (2 x 10 mL) to yield **$Fe(LPI)Cl_2$** (43.4 mg, 35.6 %). ESI (Fig. 29a): *m/z* 673.4 $[M - Cl]^+$, 319.2 $[M - 2Cl]^{2+}$.

**General procedure for a photocatalysis experiment**
The mass required for the desired **$TATA^+$** is added to a 5 mL flask. Meanwhile a stock solution of the catalyst is made up with known concentration. An aliquot of the catalyst solution is transferred into the **$TATA^+$** flask to give the desired catalyst concentration. The volume is made up to 5 mL with a 1.0 M acetic acid/acetate buffer and then transferred into a vessel of volume 180 mL which was specifically designed for photocatalysis. The required amount of SD is then added, the vessel sealed with a rubber septum and insulation tape and then covered with aluminium foil. The vessel is purged with argon for 30 minutes, or until the oxygen peak in a GC sample is too small to be integrated. The foil is then removed and the sample placed 4 cm away from a Hamamatso xenon lamp (70 % intensity, 400-700 nm filter, 40 mW $cm^{-2}$) and stirred. A 100 µL sample is withdrawn via syringe at regular intervals and injected into a GC (Perkin Elmer Autosystem XL Gas Chromatogram equipped with a 5 Å molecular sieve column (oven T = 303 K) and a thermal conductivity detector (TCD) using argon as

the carrier gas). Prior to each experiment, a calibration of the GC/TCD was performed using two samples of reference gas (1% and 5%). The peak corresponding to $H_2$ in the GC spectrum is integrated and the volume of $H_2$ ($V_{H2}$) in the headspace of the vessel calculated using Equation 1:

$$V_{H2} = \frac{peak\ area}{coefficient} \times 0.01 \times 0.175 \qquad \textit{Equation 1}$$

The coefficient is obtained from calibration of the GC for hydrogen peaks (Fig. S1). The multiplication by 0.01 is performed as the coefficient comes from calibration based off the percentage of $H_2$ in the injection. The multiplication of 0.175 is used to obtain the volume of hydrogen in litres in the headspace of the flask, which is 175 mL. The number of moles of $H_2$ ($n_{H2}$) in the headspace and the TON are calculated with Equations 2 and 3 respectively:

$$n_{H2} = \frac{V_{H2}}{24.45\ L\ mol^{-1}} \qquad \textit{Equation 2}$$

$$TON_{cat} = \frac{n_{H2}}{n_{cat}} = \frac{n_{H2}}{V_{sol} \times [Cat]} \qquad \textit{Equation 3}$$

The division by 24.5 in Equation 2 is a constant and comes from the ideal gas equation:

$$n_{H2} = \frac{pV}{RT} = \frac{101.325\ kPa \times V_{H2}}{8.314\ L\ kPa\ K^{-1}\ mol^{-1} \times 298\ K} = 0.0409\ L^{-1}\ mol \times V_{H2} = \frac{V_{H2}}{24.45\ L\ mol^{-1}}$$

**Example photocatalysis solution preparation – $TATA^+$ / 14PDN / $HA^-$ / $H_2A$ / pH 4.5**

Catalyst: **14PDN** MW = 423.65 g $mol^{-1}$ $\varepsilon_{max}$ = 380 $M^{-1}$ $cm^{-1}$ (464 nm)
Standard solution: approximately 1.0 mg in 5 mL giving A = 0.114 (1 cm cuvette) → $[Co^{III}]_o$ = 3.0 x $10^{-4}$ M
Desired $[Co^{III}]$ = 1 x $10^{-6}$ M
Volume of $[Co^{III}]_o$ added to PS flask = $C_2V_2/C_1$ = (1 x $10^{-6}$ M)(5 mL)/(3.0 x $10^{-4}$ M) = 0.167 mL

PS: **$TATA^+$** MW = 582.087 g $mol^{-1}$ $\varepsilon_{max}$ = 8800 $M^{-1}$ $cm^{-1}$ (532 nm)
Mass = 0.727 mg Volume = 5 mL [**$TATA^+$**] = 2.5 x $10^{-4}$ M

$e^-/H^+$: ascorbate/ascorbic acid (0.1 M, pH 4.5)
$[H_2A]$ = 0.05 M MW = 176.12 g $mol^{-1}$ m = 21.2 mg
[NaHA] = 0.05 M MW = 198.11 g $mol^{-1}$ m = 75.3 mg

Buffer solution: Acetic acid/sodium acetate (1.0 M 15 mL stock, pH 4.5)
[AcOH] = 0.64 M $V_{AcOH}$ = 0.5949 mL
[AcONa] = 0.36 M $m_{AcONa}$ = 442.9 mg

***Table 1:*** *Photocatalysis results for the experimental example.*

| Time / h | Area of $H_2$ peak | $V_{H2}$ in flask / L | $V_{H2}$ in flask / mL | $n_{H2}$ / mols | $TON_{cat}$ |
|---|---|---|---|---|---|
| 0 | 0.00 | 0.0000000 | 0.00 | 0.00E+00 | 0 |
| 1 | 0.39 | 0.0003166 | 0.32 | 1.29E-05 | 2590 |
| 2.17 | 0.58 | 0.0004708 | 0.47 | 1.93E-05 | 3851 |
| 4.17 | 0.71 | 0.0005764 | 0.58 | 2.36E-05 | 4715 |
| 6 | 0.75 | 0.0006088 | 0.61 | 2.49E-05 | 4980 |
| 22 | 0.87 | 0.0007063 | 0.71 | 2.89E-05 | 5777 |

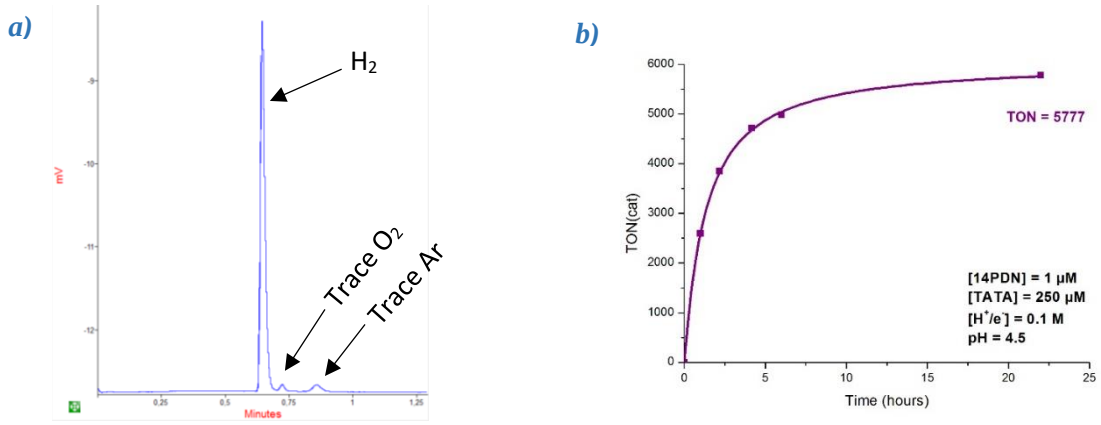


***Figure 9:*** *a) GC plot after 22h irradiation for the experimental example; b) Plot of TON vs time for the experimental example.*

**General electrochemistry procedure**

All work was performed using a three-electrode electrochemical cell under an argon atmosphere at room temperature in a glove box. 10 mL of a 0.1 M solution of $TBABF_4$ in acetonitrile was placed in the cell with a $Ag/AgNO_3$ (10 mM) reference electrode, a platinum wire auxiliary electrode and a glassy carbon working electrode (d = 3 mm). A blank CV (cyclic voltammogram) was recorded of the electrolyte solution. The mass of the product required for a 0.5 mM solution was then added, the solution stirred and then a CV recorded. The scan rate in all cases was 100 mV $s^{-1}$. Electrolyses were also performed to isolate each redox species and the UV-Vis spectrum was recorded for each species. A small amount of ferrocene was added at the end of each experiment to correct the reference.

# *IV) Results & Discussion*

## IV.1) Photocatalysis with the $TATA^+$/14PDN/$HA^-$ System

The aim of the photocatalysis experiments using the **$TATA^+$** and **14PDN** was to determine the best parameters for $H_2$ production and to hopefully explain the reasons behind some of the trends. It is worth mentioning that photocatalysis in these systems is extremely sensitive to small changes in the reaction parameters. As such, reproducibility is often difficult and requires many repeats; the results included in this report are the most concordant results obtained. TONs should not be taken as absolute values and rather the trend in TONs should be the important consideration. Slight changes in factors such as photon flux from the lamp, temperature, amount of $O_2$ in the reaction vessel, weighing of components, and many more could have a large effect on the outcome of the system. Many sets of photocatalysis data were obtained (see Table S1).

### *IV.1.a) Electrochemical Properties of $[Ru(bpy)_3]^{2+}$ and $TATA^+$ and Mechanistic Insight*

Extensive studies of **Ru** in association with **14PDN** have already been carried out by CIRE which will serve as a comparison for **$TATA^+$**.[45,56] Upon photoexcitation, an initial $^1$MLCT state is populated to generate $[Ru^{III}(bpy^{\bullet-})(bpy)_2]^{2+}$ (denoted $^{1*}\mathbf{Ru^{II}}$) which rapidly undergoes *isc* (intersystem-crossing) to a $^3$MLCT state ($^{3*}\mathbf{Ru^{II}}$). In the RQP, $^{3*}\mathbf{Ru^{II}}$ is reduced to $[Ru^{II}(bpy^{\bullet-})(bpy)_2]^+$ (denoted $\mathbf{Ru^{I}}$) by $HA^-$, followed by an electron transfer from $bpy^{\bullet-}$ to **14PDN**. Fig. 10 demonstrates why **Ru** is a good photosensitizer regardless of which quenching pathway is taken. $^{3*}\mathbf{Ru^{II}}$ is both a better reducing and oxidising agent than **Ru** as the ionisation energy (IE) is smaller and the electron affinity (EA) is larger. To perform as an efficient photosensitizer, the reduced species also needs to have a reduction potential low enough to provide a thermodynamic driving force for the electron transfer to the catalyst. For the electron transfer to be thermodynamically favourable, ΔG must be negative. This can be calculated in eV from the difference in reduction potentials. The redox couple $E(\mathbf{Ru^{II}}/\mathbf{Ru^{I}})$ has a reduction potential of -1.50 V (in $H_2O$, *vs* SCE) meaning that $\mathbf{Ru^{I}}$ is a powerful reductant. The $E(Co^{II}/Co^{I})$ redox couple for **14PDN** has a reduction potential of -0.85 (in $H_2O$, *vs* SCE). Therefore, ΔG for the electron transfer is -0.65 eV and it is thermodynamically favourable.

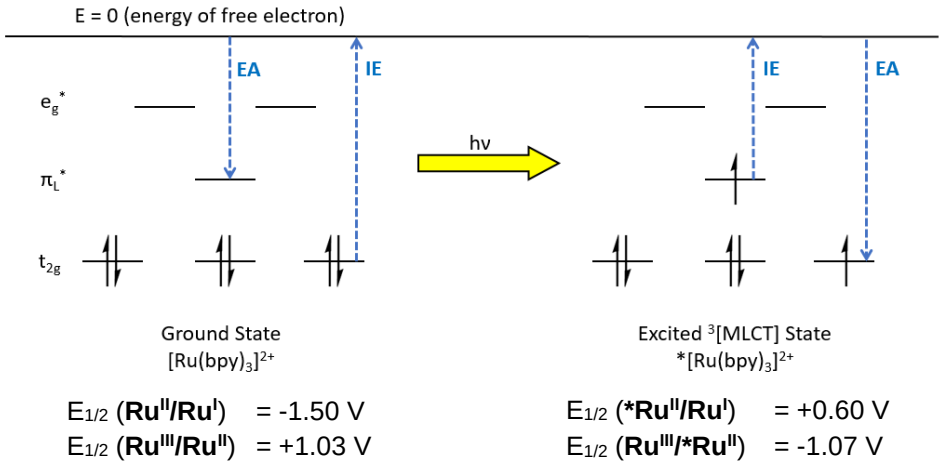


***Figure 10:*** *HOMO/LUMO energy levels and redox potentials of* ***Ru*** *(in $H_2O$ vs SCE).*[3]

Recent electrochemical studies of **TATA**$^+$ by CIRE have demonstrated why it can succesfully be used as a photosensitizer with **14PDN**. The CV of **TATA**$^+$ (Fig. 11) exhibits two successive one-electron reduction processes at -1.48 V and -2.1 V (*vs* $Ag/AgNO_3$) in MeCN + 0.1 M $TBABF_4$. These potentials can be converted to the SCE by adding ~300 mV. This therefore corresponds to reversible reductions at -1.18 V and -1.8 V *vs* SCE for the redox couples E(**TATA**$^+$/**TATA**$^\bullet$) and E(**TATA**$^\bullet$/**TATA**$^-$) respectively. The electron transfer from **TATA**$^\bullet$ to **14PDN** is thermodynamically favourable as $\Delta G = -0.33$ V, however less so than from $\mathbf{Ru^I}$. The shape of the waves indicate that the first reduction is fully reversible but the second is only quasi-reversible. The reversibility of the first reduction process was demonstrated via reversible bulk solution electrolysis.

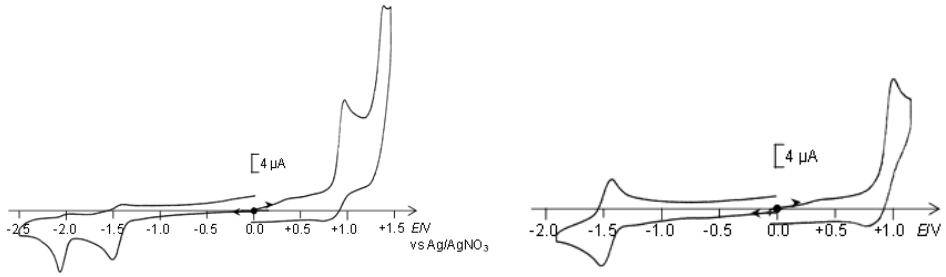


***Figure 11:*** *CVs of* ***TATA***$^+$ *in MeCN + 0.1 M $TBABF_4$ referenced against $Ag/AgNO_3$ with a glassy carbon (d = 3 mm) working electrode and a platinum wire auxiliary electrode.*

Upon photoexcitation, **TATA**$^+$ forms a singlet excited state (**TATA***). The absence of a heavy atom effect means that *isc* to the triplet state does not occur. This is supported by the short lifetime ($\tau$) of 14 ns as determined by photophysical studies. Triplet states have much longer lifetimes as phosphorescence is a spin-forbidden process, for example the lifetime of $^3\mathbf{*Ru^{II}}$ is 630 ns in water.[68] However, the short lifetime of **TATA*** does not impede the catalysis as electron transfer from $HA^-$ occurs on a much faster timescale (this has been demonstrated by CIRE using nanosecond transient absorption spectroscopy). It is hypothesized that excitation of **TATA**$^+$ involves charge transfer from a nitrogen atom to the carbocation to form a radical cation on the nitrogen and a delocalised radical on the carbon framework. Reduction of **TATA*** by $HA^-$ would therefore reduce nitrogen radical to generate **TATA**$^\bullet$ (Fig. 12). CIRE have also demonstrated the occurrence of a RQP

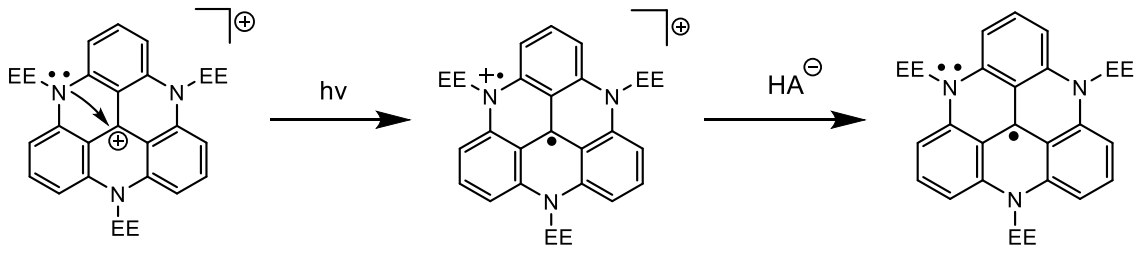


***Figure 12:*** *Hypothesized formation of* ***TATA***$^\bullet$.

using Stern-Volmer plots to show that $HA^-$ is a better quencher of **TATA*** than **14PDN** ($1.23 \times 10^{10}$ $M^{-1}$ $s^{-1}$ *vs* $3.59 \times 10^9$ $M^{-1}$ $s^{-1}$).

Previous studies of **14PDN** and similar cobalt complexes of the type $[Co(N4Py)(X)]^{n+}$ (N4Py = 1,1-di(pyridin-2-yl)-N,N-bis(pyridin-2- ylmethyl)methanamine) have provided an insight into the mechanism of $H_2$ generation which can be applied to this system (Fig. 13).[45,56,69] The $Co^I$ species, formed by reduction from **TATA$^\bullet$**, adopts a square-based pyramid or a square planar geometry via loss of one or two axial $H_2O$ ligands respectively. $Co^I$ is then protonated to form a $Co^{III}$-H hydride species from which there are three possible pathways (Fig. 13). It has been hypothesized that reduction by a $Co^I$ species (or **TATA$^\bullet$**) is the most favourable and that $H_2$ is predominantly generated from reaction of two $Co^{II}$-H species to regenerate the $Co^I$ species, or reaction of one $Co^{II}$-H with $H^+$ to regenerate the $Co^{II}$ species. In any case, the active catalytic species present in solution is $[Co^{II}(CR)(H_2O)_2]^{2+}$ and two molecules of **TATA$^\bullet$** are needed overall.

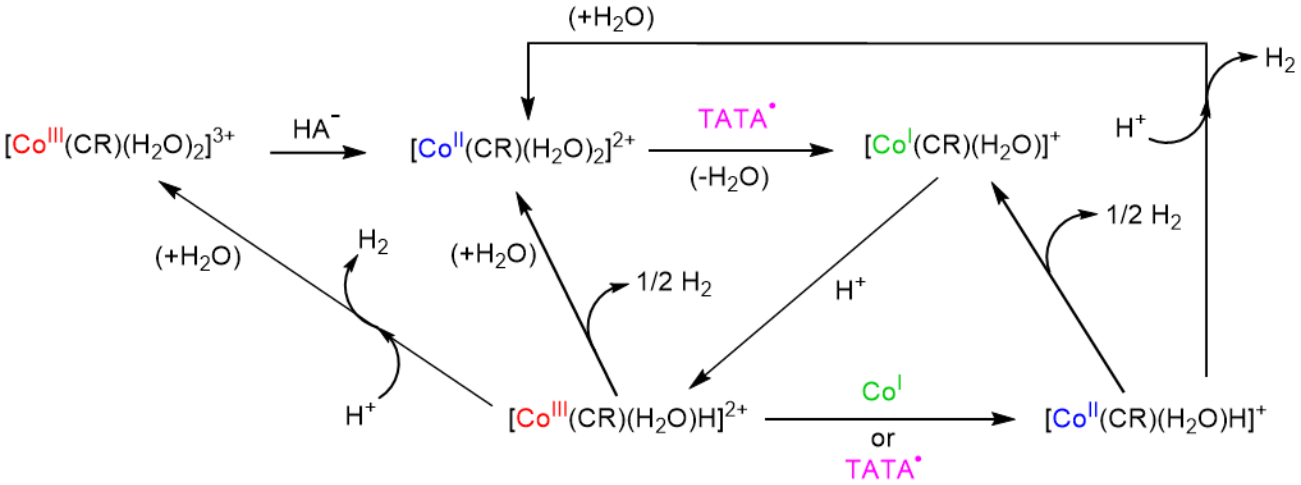


***Figure 13:*** *Possible catalytic pathways to $H_2$ production with **TATA$^+$**, **14PDN**, and $HA^-$.*

### *IV.1.b) Variation of pH*

The pH of a photocatalytic system is very important and is often a balance between quenching of PS* and formation of the active metal-hydride (M-H). At high pH, the deprotonated form of the PS predominates and so quenching of PS* is very efficient as the SD is a stronger reductant. However, the concentration of protons in solution is low meaning that the catalysis is limited by slower formation of M-H. At low pH the opposite is true; M-H is easily formed but quenching of PS* is limited because the SD is protonated. For this reason, ascorbate is a good SD at acidic pH because it remains deprotonated and therefore a strong reductant. Other SDs such as TEOA and TEA cannot function in acidic conditions as they are protonated and therefore not donating enough.

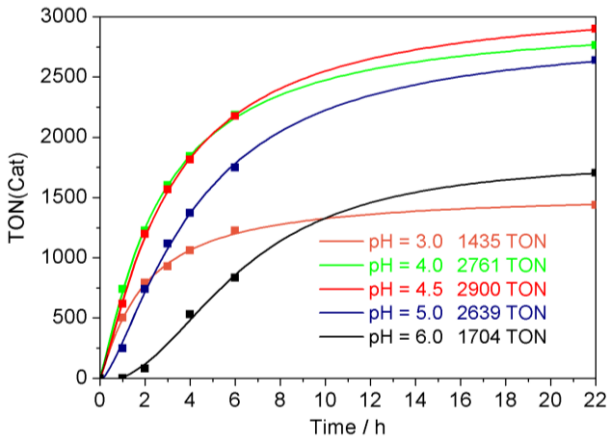


***Figure 14:*** *Plot of $TON_{Cat}$ vs time for photocatalysis using **TATA$^+$** (500 μM) at varying pH with **14PDN** (10 μM) in 5 mL deaerated aqueous solutions containing $HA^-/H_2A$ (0.1 M) and a 1.0 M acetate buffer.*

The pH dependence of photocatalysis with **TATA**$^+$ was tested under typical photocatalysis conditions. As shown in Fig. 14, pH 4.5 was found to be the most effective and confirms that **TATA**$^+$ is a stable photosensitizer under acidic aqueous conditions.

### *IV.1.c) Variation of [TATA$^+$]*

The [**TATA**$^+$] was varied to determine the best concentration at pH 4.5 (Fig. 15). The peak TON value with **TATA**$^+$ is different to that of the **Ru** system where 500 µM is the best concentration. For **TATA**$^+$, the maximum TON peaks at a concentration of 250 µM at which roughly 50 % more $H_2$ is produced compared to higher or lower concentrations. The increase in TON from 100 µM to 250 µM can be explained by a phenomenon observed in all photocatalytic systems: increasing the PS:Cat ratio effectively increases the concentration of **TATA**$^\bullet$ surrounding each **14PDN** complex and therefore formation of the active metal-hydride is less limited by the amount of **TATA**$^\bullet$ in solution.

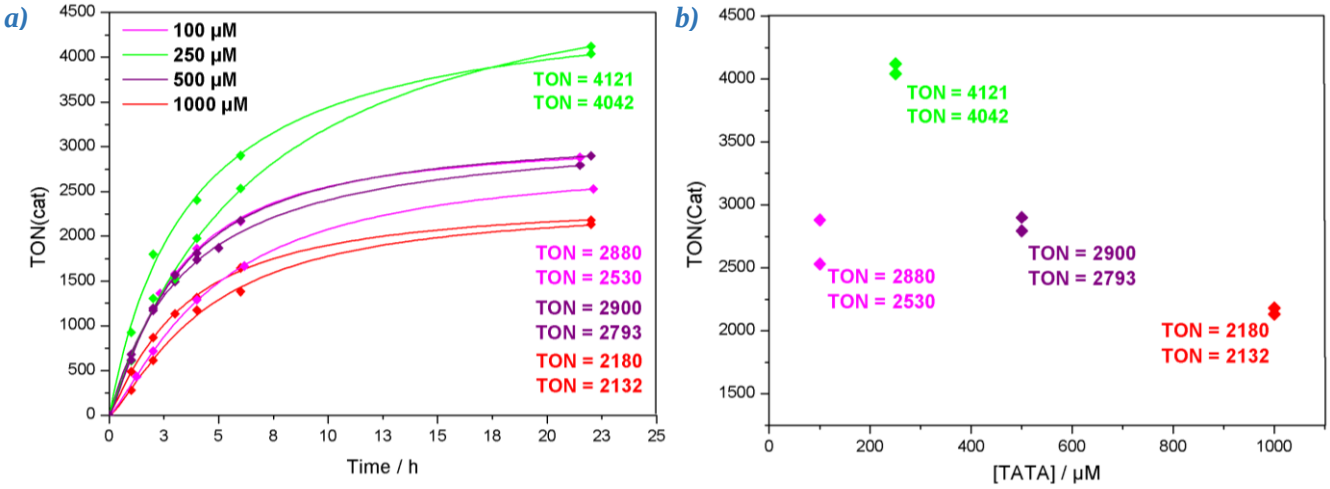


***Figure 15:*** *Effect of varying the concentration of* ***TATA***$^+$ *at a fixed concentration of* ***14PDN*** *(10 µM) in 5 mL deaerated aqueous solutions containing $HA^-/H_2A$ (0.1 M) and a 1.0 M acetate buffer (pH 4.5).*

Why is a decrease in TON with increasing [**TATA**$^+$] from 250 µM to 1 mM observed? Π-stacking at high concentrations is one hypothesis; this occurrence in **TATA**$^+$ should hinder the photocatalysis by isolating individual molecules from the catalyst. To test this hypothesis, UV-visible absorption spectra were taken of aqueous solutions of **TATA**$^+$ with varying concentrations up to 2 µM (Fig. 16). If π-stacking is occurring, a linear dependency of absorption and concentration will not be observed as the π-stacking would affect the absorption at higher concentrations. However, the results show that π-stacking of **TATA**$^+$ is not responsible for

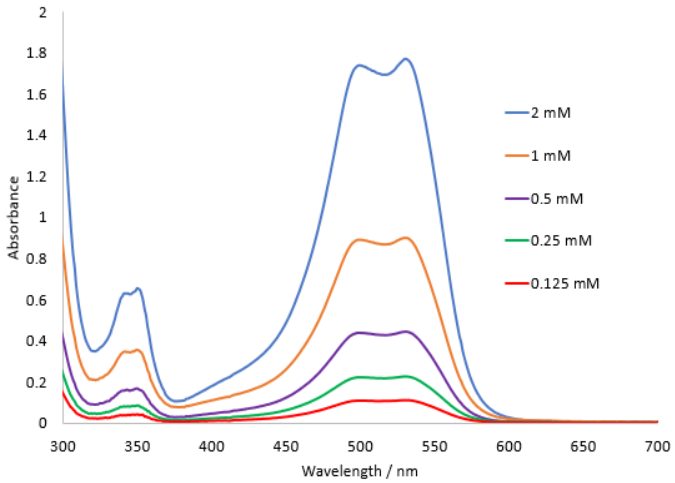


***Figure 16:*** *UV-visible spectra of solutions with varying concentrations of* ***TATA***$^+$ *in $H_2O$ (l = 1 mm).*

the decrease in activity at concentrations up to 2 mM. The loss in activity is therefore likely due to the high concentration of **TATA**$^+$ blocking/scattering the incoming light which means that the molecules in the solution furthest from the lamp receive less irradiation. However, this does not explain why the TON peaks at a lower concentration than that of **Ru** when **Ru** has a larger $\varepsilon_{max}$. Another possibility is that the emission of **TATA*** could produce a filtering effect and destructively interfere with some of the incoming irradiation. More work is needed to discover the origin of this observation.

### *IV.1.d) Variation of [14PDN]*

Knowing the best [**TATA**$^+$], the [**14PDN**] was varied to observe the effect. The concentration of catalyst should always be a consideration when developing photocatalytic systems as it is usually a balance between high TONs and overall volume of $H_2$ produced. Theoretically, the [Cat] should not affect the TON because the moles of $H_2$ and [Cat] should scale linearly. However this is not the case as larger TONs are achieved at lower catalyst concentrations. This is a phenomenom seen in practically all photocatalytic TCSs, the origin of which comes from the fact that at lower catalyst concentrations there is a larger percentage of active catalyst complexes. Fig. 17 shows the effect of varying [**14PDN**] for systems with 250 μM of **TATA**$^+$. As expected, the general trend is an increase in TON with decreasing [**14PDN**]. Interestingly, the PS/Cat ratio phenomenom does not apply between concentrations of 5 and 10 μM of **14PDN** as both concentrations result in the same TON. Despite the high TONs achieved at 1 μM of **14PDN**, decreasing the concentration any lower than this is not desirable as the volume of $H_2$ would become insignificant.

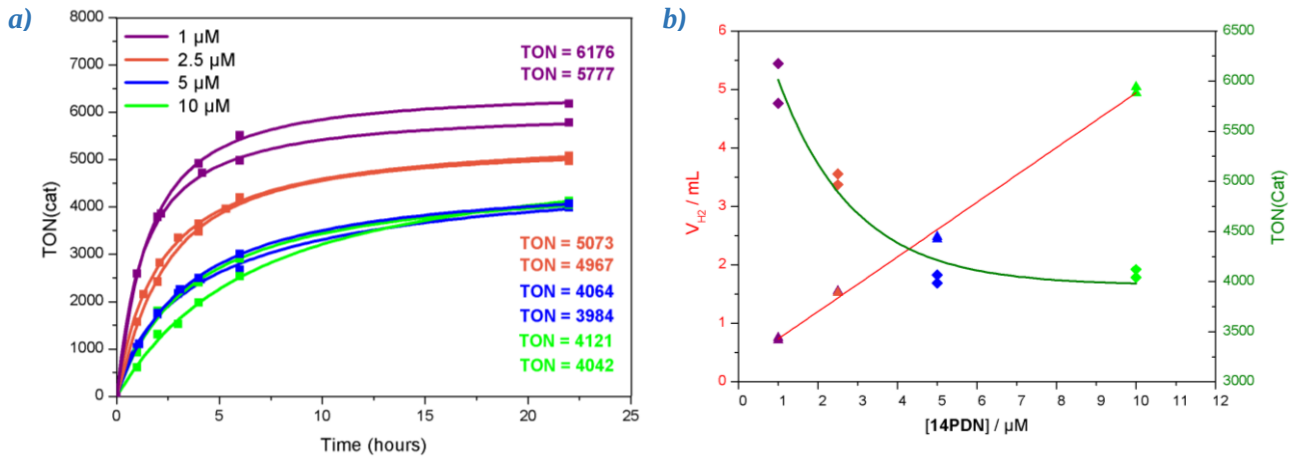


***Figure 17:*** *Effect of varying the concentration of **14PDN** at a fixed concentration of **TATA**$^+$ (250 μM) in 5 mL deaerated aqueous solutions containing $HA^-/H_2A$ (0.1 M) and a 1.0 M acetate buffer (pH 4.5).*

### *IV.1.e) Test for Homogeneity by Mercury Poisoning*

It is well known that proton reduction can be carried out by metallic colloidal particles and that aggregation of catalyst complexes to form redox-active colloids is known to occur.[70] Mercury poisoning is a common test to determine whether the catalysis is homogeneous. Adding a few drops of mercury into the reaction mixture will trap the colloids if they are present as the mercury attaches onto their surfaces, thus preventing catalysis. This test was carried out on a solution with 500 μM of **TATA** and 10 μM of **14PDN** to observe whether the TON was affected (Fig. 18). The results indicate that catalysis in this system is homogeneous as the reaction

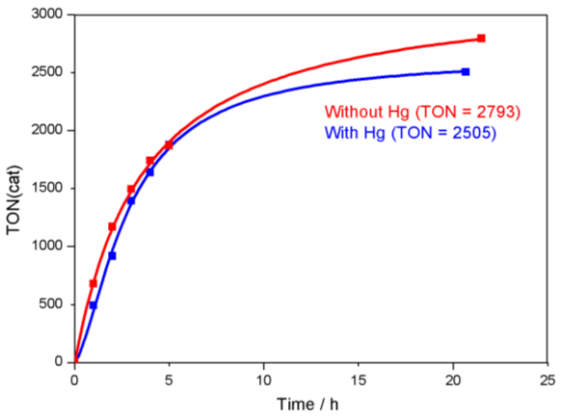


***Figure 18:*** *Plots of $TON_{Cat}$ vs time in the presence and absence of mercury in identical conditions (500 μM **TATA**$^+$, 10 μM **14PDN**, 0.1 M $HA^-/H_2A$ at pH 4.5).*

profile is almost identical. Another technique commonly used to test for homogenenity is dynamic light scattering in which the amount of scattered light passing through the solution is measured and therefore the amount of colloidal matter can be determined.

### *IV.1.f) Performance vs $[Ru(bpy)_3]^{2+}$ and Stability*

Decomposition of a photosensitizer results in a loss in absorption and therefore deactivation of the system (known as bleaching). It is well known that inorganic and organic photosensitizers suffer from decomposition of their reduced radical state that is formed via reductive quenching.[8,63,71] Dyes such as **RB** and **EY** contain halogenated rings to facilite *isc* to a triplet state through the heavy atom effect, however cleavage of the C-X bonds contributes to their decomposition. Inorganic photosensitizers can suffer from ligand loss or reorganisation, coordination of the solvent, and all photosensitizers are potentially succeptible to hydrogenation. Of course, the activity of a photosensitizer is related to its resistance to these deactivation processes.

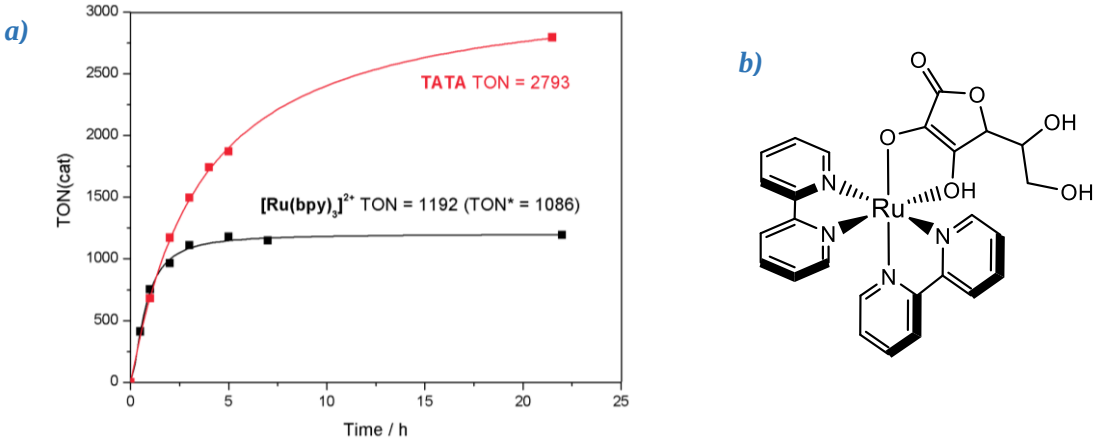


***Figure 19:*** *a) Comparison of photocatalytic activity of* ***TATA***$^+$ *and* ***Ru*** *(500 μM) with* ***14PDN*** *(10 μM) + 0.1 M* $HA^-/H_2A$ *at pH 4.5. TON* is the TON corrected for the* $H_2$ ***Ru*** *produces in absence of* ***14PDN****. b) Decomposition product of* ***Ru*** *in the presence of ascorbate.*

The photocatalysis results also demonstrated that **TATA**$^+$ is a better photosensitizer than **Ru** when used in association with **14PDN** (Fig. 19a). For example, **Ru** reaches a TON of 1086 at a concentration of 500 μM and 10 μM of **14PDN** *vs* ~2800 with **TATA**$^+$. The reason for this can be attributed to the greater stability of **TATA**$^+$ compared to **Ru** in aqueous acidic conditions, as can be demonstrated by UV-Vis spectroscopy (Fig. 20). When a solution of **Ru** (500 μM) in the presence of 0.1 M $HA^-/H_2A$ at pH 4.5 was irradiated in the absence of **14PDN**, the absorption peak at 450 nm had decreased by roughly 50 % after 24 h and $\lambda_{max}$ had shifted suggesting

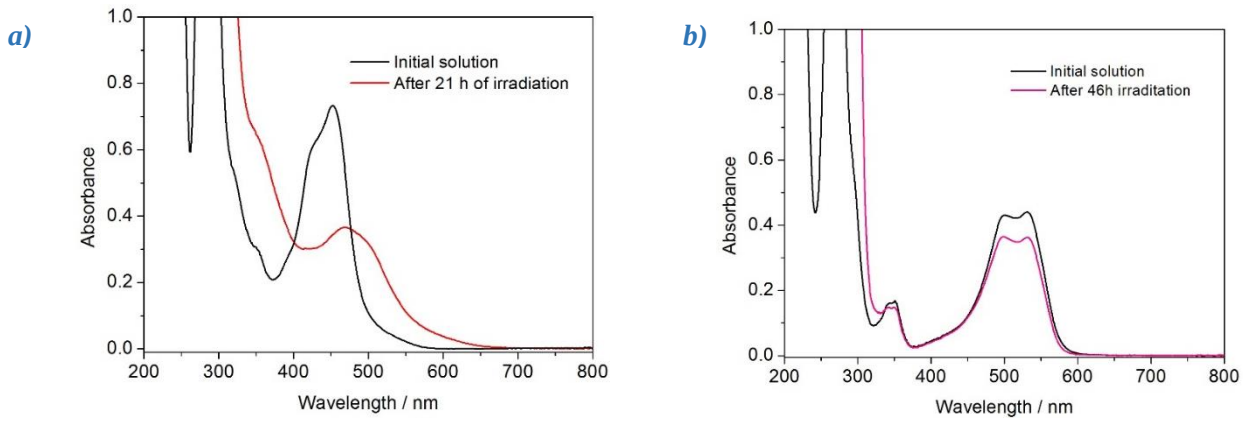


***Figure 20:*** *UV-Visible spectra before and after irradiation of a 500 μM solution of* ***Ru*** *(a) and* ***TATA***$^+$ *(b) in 0.1 M* $HA^-/H_2A$ *at pH 4.5. Increased absorption of the final solutions at wavelengths 300 nm or less is due to the presence of ascorbate which is not present at the time of recording the spectrum of the initial solution.*

complete transformation of **Ru** into another species. The identity of this species has been shown to be ruthenium coordinated by two bipyridine ligands and an ascorbate molecule (Fig. 19b).[63] A solution of **TATA**$^+$ under the same conditions showed very little bleaching after 46 h of irradiation. The better stability is manifested into an increased longevity of the system; $H_2$ is produced for up to 22 h with a plateau starting around 6 h for **TATA**$^+$, whereas in similar conditions the photocatalysis is complete by 4-5 h when **Ru** is used.

The high stability of **TATA**$^+$ can be accounted for by looking at the structure. **TATA**$^\bullet$ has a large degree of delocalisation of the radical around the aromatic rings and the presence of three electron-donating nitrogens also stabilize the radical. This delocalisation lowers the possibility of potential decomposition pathways via radical combination, such as dimerization of two **TATA**$^\bullet$ radicals. Despite the higher TON with **TATA**$^+$, the systems with **Ru** usually exhibit slightly higher initial TOFs as seen from the steeper initial gradient. This means that **Ru** has an inherently higher activity than **TATA**$^+$ but is less stable. The higher activity is not surprising given the lower reduction potential of **Ru**.

Despite the high stability of **TATA**$^+$, slight bleaching of the solution still occurs and a small decrease of the absorption peak is observed by the end of the catalysis. Fig. 21 shows a typical decrease of the absorption peaks for **TATA**$^+$ in the UV-visible spectra obtained over 22h of a photocatalysis. The exact route of decomposition is unknown but it is hypothesized that **TATA**$^+$ or **TATA**$^\bullet$ is hydrogenated during the photocatalysis.

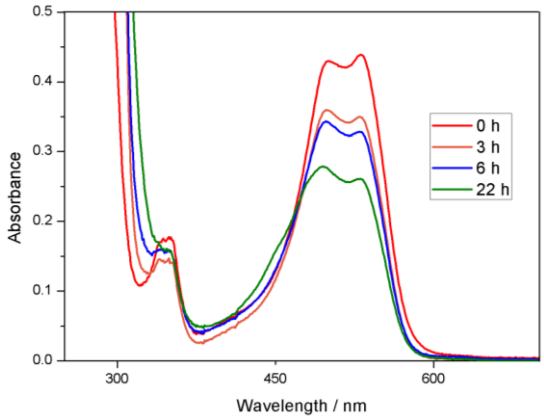


***Figure 21:*** *UV-Visible spectra of a 500 µM solution of* ***TATA***$^+$ *with* ***14PDN*** *(10 µM) in 5 mL deaerated aqueous solutions containing* $HA^-/H_2A$ *(0.1 M) and a 1.0 M acetate buffer (pH 4.5).*

## IV.2) Synthesis of New Tetraaza Polypyridine-(bis)imine Co and Fe Complexes

### *IV.2.a) Ligand Synthesis*

The first step in the synthesis of the ligands is formation of the diacetyl compounds **L1** and **L2** from the dibromo or dichloro precursors following literature procedures (Figs. 22a, 22b).[72,73] Synthesis of **L1** was carried out in two steps. The first involved a Stille coupling using a tributyl-tin catalyst to form an ethoxy-vinyl substituted phenanthroline. The second step was an acid hydrolysis to yield **L1**. Both the ethoxy-vinyl intermediate and **L1** were purified on alumina columns and evidence for both products can be seen from their $^1$H NMR spectra which correspond to those reported in the literature (Figs. S2 and S3).

The first step in the synthesis of **L2** involved a halogen-lithium exchange on the bipyridine using the strong base $^n$BuLi. Any traces of water in the solvent can quench the base and prevent this step from occuring. The lithiated bipyridine then attacks the amide of DMA and an acid/base workup is used to release the amine and neutralise the pH. **L2** was purified by recrystallization from hot ethanol and evidence from the product can be seen from it's $^1$H NMR peaks which correspond to those reported in the literature (Fig. S4).

The amine 2,6-diisopropylaniline was planted onto the diacetyl compounds to form the polypyridine-(bis)imine ligands **LBI** and **LPI**. **LBI** was synthesised according to literature procedure and the same procedure was used to synthesise **LPI** which has not yet been reported.[66] The synthesis was a straightforward

condensation reaction that was able to use the amine as a solvent in a neat rection, and formic acid was added to facilitate the condensation by protonating the ketone. Evidence for the formation of **LBI** can be seen from the $^{1}$H NMR and mass spectra (Figs. S8 and S9). Being a new compound, there is no literature characterization data to comapare against for **LPI**, however both the $^{1}$H NMR and mass spectra are as expected. Both show characteristic peaks for the C=N stretching vibrations of the imine in the IR spectra around 1670 cm$^{-1}$ and the absence of C=O stretching vibrations around 1900 cm$^{-1}$.

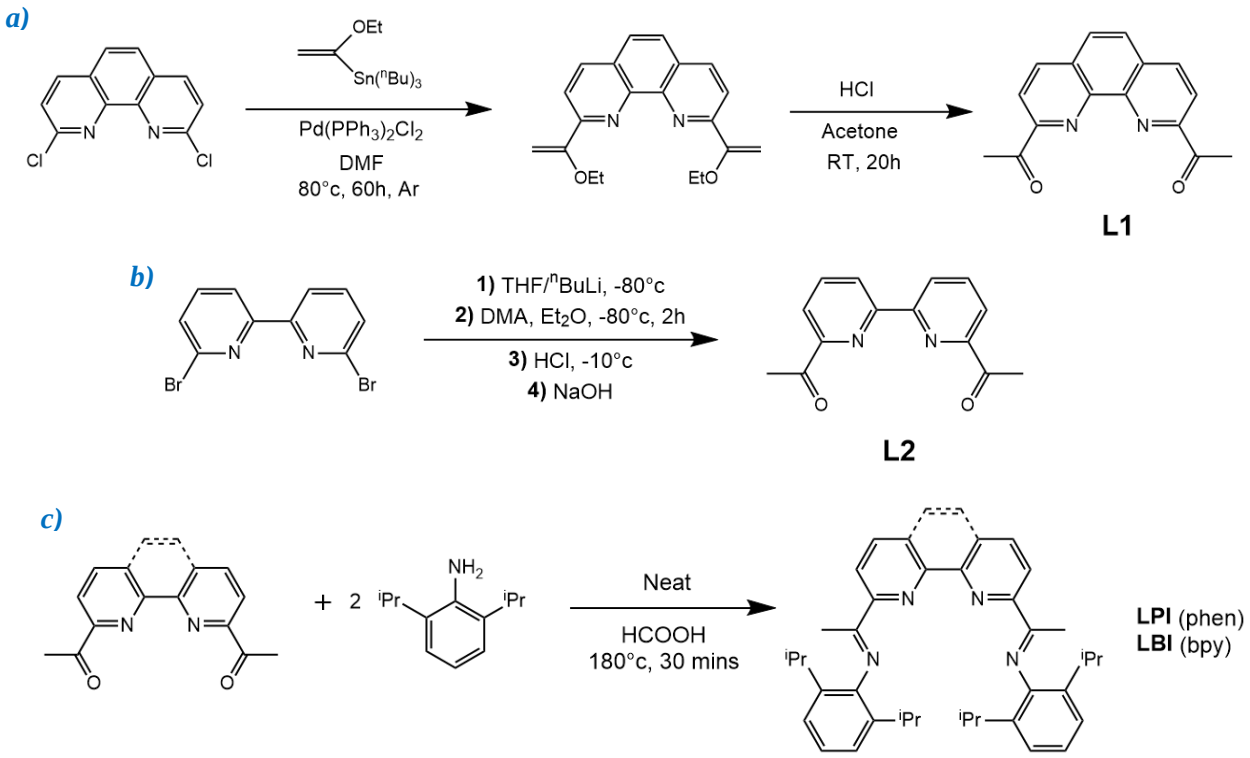


***Figure 22:*** *a) Synthesis of 2,9-diacetylphenanthroline, b) Synthesis of 6,6-diacetyl-2,2'-bipyridine; c) Formation of the (bis)imine ligands. DMA = dimethylacetamide.*

### *IV.2.b) Synthesis and Electrochemical Studies of the Complexes*

Herein is reported the synthesis and electrochemical study of a cobalt complex [Co$^{II}$(LPI)(MeCN)$_2$](BF$_4$)$_2$ (denoted **CoLPI)**. The stirring of **LPI** with Co(BF$_4$)$_2$.6H$_2$O in acetonitrile at 70°c for 4 h gave an orange solution which, upon cooling and additon of Et$_2$O, yielded **CoLPI** as a deep yellow-coloured solid in a 95% yield. The $^{1}$H NMR spectrum is consistent with a paramagnetic Co$^{II}$ complex as no complex or ligand peaks are observed due to fast relaxation of the nuclear spins. The absence of current in the CV at 0V demonstrates the stability of the Co$^{II}$ species (Fig. 24a). Identifiable peaks were found in the mass spectrum (Fig. S12). The IR spectrum exhibits similar peaks as the ligand with an additional peak at 1084 cm$^{-1}$ for BF$_4$ vibrations of the counter-ion. Presence of axial MeCN ligands from the solvent is supported by the peaks at 2309 and 2281 cm$^{-1}$ which are consistent with the fundamenetal C-N stretching frquency of a nitrile coordinated to a cobalt centre.[74] The stretching frequency of coordinated MeCN is slightly higher than the fundametnal stretching frquency of free MeCN. This is because σ-donation of electron density to the Lewis-acidic cobalt is from the nitrogen lone pair which has some antibonding character. Removal of electron density from this orbital increases the strength of the the C-N bond.

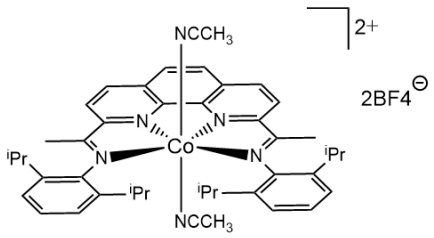


***Figure 23:*** *Proposed structure of **CoLPI**.*

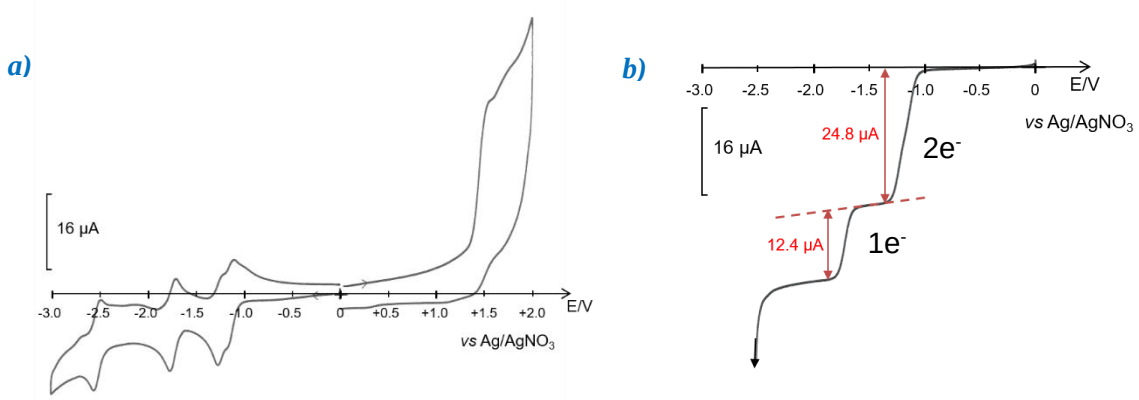


***Figure 24:*** *a) CV of 0.5 mM **CoLPI** in MeCN + 0.1 M $TBABF_4$; b) Linear sweep voltammogram of 0.5 mM **CoLPI** in MeCN + 0.1 M $TBABF_4$ using a rotating carbon disk electrode at 120 rpm scanning at 10 mV/s.*

The CV of **CoLPI** (Fig. 24a) exhibits four reversible reduction processes at -1.14, -1.26, -1.75 and -2.54 and one irreversible oxidation process at +1.60 *vs* $Ag/AgNO_3$. The first two reduction processes are overlapping as they occurs at very close potentials. A rotating disk electrode was used to prove that this wave is due to a two-electron process as the height of the first plateau is twice that of the second (Fig. 24b). The complex is stable to oxidation to $Co^{III}$ in air as the $E(Co^{III}/Co^{II})$ redox couple is seen as an irreversible peak at +1.60 V. Exhaustive bulk electrolysis to -1.5 V afforded a colour change from yellow to green to brown which futher supports a two electron reduction. At -1.5 V the CV was almost identical indicating the excellent reversibility of the first two reduction processes (Fig. 25a). Electrolysis to -1.85 V was also performed but no change in colour was observed. Interestingly, at -1.85 V the first two reduction processes become more distinct (Fig. 25b). Electrolysis back to +0.00 V regenerated a yellow solution which exhibited two new reversible processes (Fig. 25d).

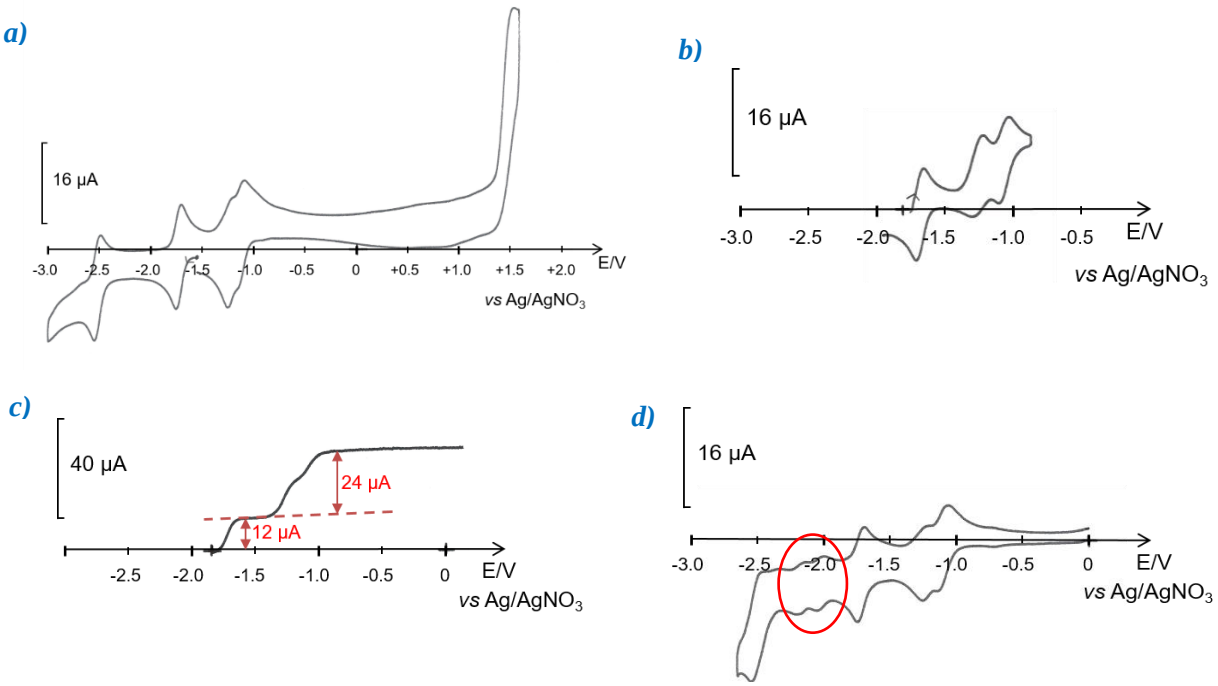


***Figure 25:*** *a) CV of 0.5 mM **CoLPI** in MeCN + 0.1 M $TBABF_4$ after an exhaustive electrolysis to -1.50 V (Q = -1.29 C); b) CV of 0.5 mM **CoLPI** in MeCN + 0.1 M $TBABF_4$ after an exhaustive electrolysis to -1.85 V (Q = -0.74 C); Linear sweep voltammogram of 0.5 mM **CoLPI** in MeCN + 0.1 M $TBABF_4$ using a rotating carbon disk electrode at 120 rpm scanning at 10 mV/s after an exhaustive electrolysis to -1.85 V; d) CV showing new processes of 0.5 mM **CoLPI** in MeCN + 0.1 M $TBABF_4$ after returning to +0.00 V via an exhaustive electrolysis (Q = +1.49 C).*

EPR spectra of the initial solution and the solutions after each bulk electrolysis were recorded to help assign the redox processes (Fig. 26a). The spectrum of the initial solution containing $Co^{II}$ is typical of a high-spin $Co^{II}$ $d^7$ configuration with S = 3/2 when recorded at temperatures higher than 10 K.[74] Fast relaxation of the spins under the EPR experimental conditions (T = 100 K) results in excessive broadening of the signal, a typical observation for systems with S > 1/2. This signal can only be properly seen if recorded at a very low temperature (< 10 K). A low-spin $d^7$ configuration with S = 1/2 can be ruled out as it would have displayed an observable peak at 100 K with hyperfine coupling to the nuclear spin of Co ($A_{Co}$ = 7/2). After the bulk electrolysis to -1.50 V, a signal is observed. The signal suggests that the two-electron reduction has lead to radical anions on imine units. The five unpaired electrons in the system (three on cobalt, two on the ligand) align in an antiparallel fashion to give S = 1/2. Had one of the reductions been metal-centred to produce $Co^{I}$ and $N^{\bullet-}$, the EPR spectrum would be much more complicated due to hyperfine coupling of the unpaired electron with the nuclear spins of N ($A_N$ = 1) and Co. In fact, it has been reported that in similar complexes, two-electron reductions lead to carbon (rather than nitrogen) radicals (Fig. 26b).[75] It is therefore assumed that the $E(Co^{II}/Co^{I})$ redox couple occurs at -1.75 V and that any processes after that are phenanthroline reduction processes. At -1.85 V, the $Co^{I}$ species with 2 x $N^{\bullet-}$ is silent in EPR.

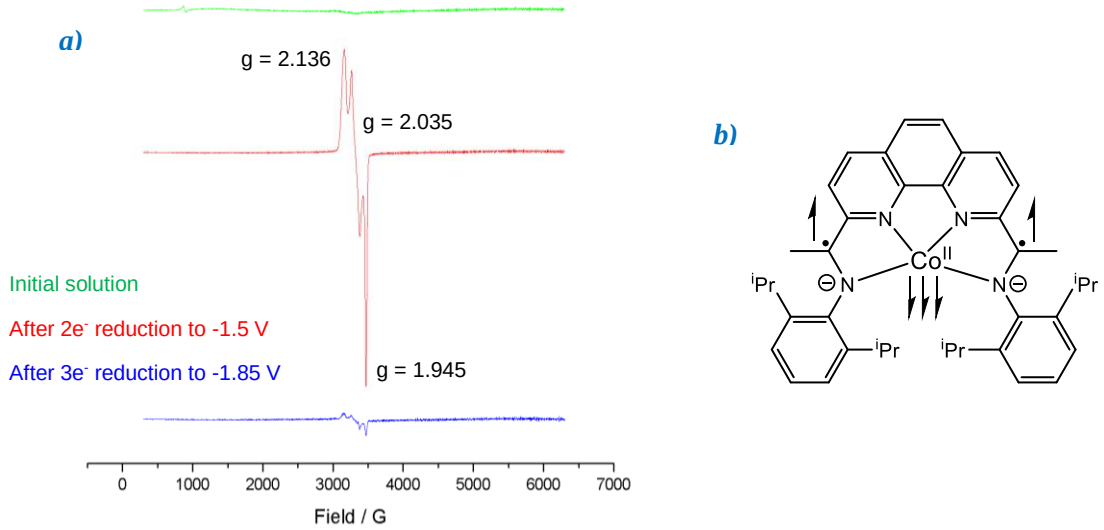


***Figure 26:*** *a) EPR spectra (100 K) of solutions of **CoLPI** before bulk electrolysis (green), after a 2e⁻ bulk electrolysis to -1.5 V (red), and after a further 1e⁻ reduction to -1.85 V (blue); b) Proposed identity of **CoLPI** after a two-electron reduction.*

The low potential for the $E(Co^{II}/Co^{I})$ redox couple of **CoLPI** means that it would not be a compatible catalyst with **TATA**$^+$; in fact this process is more negative than E(**TATA**$^+$/**TATA**$^{\bullet}$). Potentially, it could be used in association with **Ru** which is a stronger reductant than **TATA**$^+$ by ~300 mV. To increase the reduction potential of **CoLPI** electron-withdrawing groups could be incorporated into the *para* position of the diisopropyl phenyl groups. This would remove electron density from the imine nitrogen donors and make them less donating to the cobalt.

Herein is also reported the synthesis and electrochemical study of three iron complexes: $[Fe(LPI)(EtOH)_2](BF_4)_2$, $[Fe(LBI)(EtOH)_2](BF_4)_2$ (denoted **FeLPI** and **FeLBI**), and **[Fe(LPI)Cl$_2$]**. **FeLPI** and **FeLBI** were obtained as purple solids after heating **LPI** and **LBI** in ethanol with $Fe(BF_4).6H_2O$ overnight.

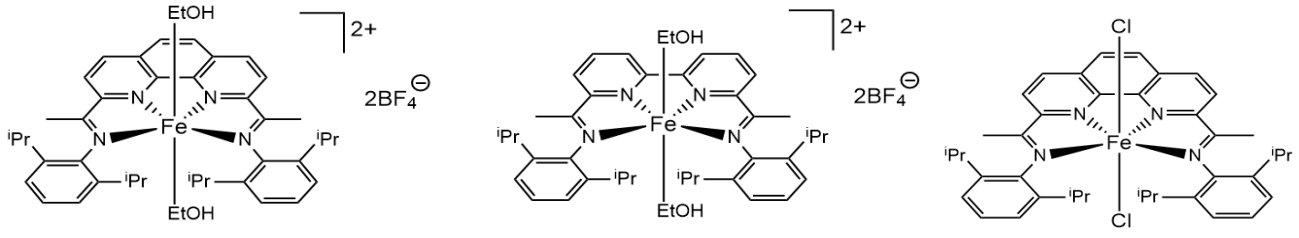


***Figure 27:*** *Proposed structures of **FeLPI**, **FeLBI** and **[Fe(LPI)Cl$_2$]**.*

***Table 2:*** *Redox potential data. CVs recorded at 0.5 mM of complex in MeCN + 0.1 M $TBABF_4$ referenced against $Ag/AgNO_3$ with a glossy carbon working electrode and a platinum wire auxiliary electrode.*

| Compound | Process | $E_{p,c}$ / V | $E_{p,a}$ / V | $E_{1/2}$ / V ($\Delta E_p$ / mV) *vs* $Ag/AgNO_3$ | $E_{1/2}$ / V *vs* SCE |
|---|---|---|---|---|---|
| **CoLPI** | $Ox_1$ | - | +1.60 | - | - |
| | $Red_1$ | -1.18 | -1.10 | -1.14 (80) | -0.84 |
| | $Red_2$ | -1.30 | -1.22 | -1.26 (80) | -0.96 |
| | $Red_3$ | -1.78 | -1.72 | -1.75 (60) | -1.45 |
| | $Red_4$ | -2.58 | -2.50 | -2.54 (80) | -2.24 |
| **FeLPI** | $Ox_1$ | +0.74 | +0.82 | +0.77 (80) | +1.07 |
| | $Red_1$ | -1.14 | -1.00 | -1.07 (140) | -0.77 |
| | $Red_2$ | -1.64 | -1.60 | -1.62 (40) | -1.32 |
| | $Red_3$ | -1.82 | -1.74 | -1.78 (80) | -1.48 |
| | $Red_4$ | -2.08 | -1.98 | -2.03 (100) | -1.73 |
| **FeLBI** | $Ox_1$ | +0.60 | +0.70 | +0.65 (100) | +0.95 |
| | $Red_1$ | -1.20 | - | - | - |
| | $Red_2$ | -2.14 | -2.06 | -2.10 (80) | -1.80 |
| | $Red_3$ | -2.30 | - | - | - |
| **[Fe(LPI)$Cl_2$]** | $Ox_1$ | +0.36 | +0.40 | +0.38 (40) | +0.68 |
| | $Ox_2$ | +0.96 | +1.10 | +1.13 (140) | +1.43 |
| | $Red_1$ | -0.34 | -0.26 | -0.30 (80) | 0.00 |
| | $Red_2$ | -1.28 | -1.20 | -1.24 (80) | -0.94 |
| | $Red_3$ | -1.68 | -1.60 | -1.64 (80) | -1.34 |
| | $Red_4$ | -1.82 | -1.74 | -1.78 (80) | -1.48 |
| | $Red_5$ | -2.06 | -1.94 | -2.00 (120) | -1.70 |

Presence of $Fe^{II}$ is supported by the oxidation waves to $Fe^{III}$ seen in the CVs (Figs. 28a and 28b), and the slow oxidation to $Fe^{III}$ in air (demonstrated by the colour change of solutions of **LPI** and **LBI** from purple to brown). The $^1H$ NMR spectrum of **FeLBI** and **FeLPI** did not show any peaks due to the paramgnetism of high-spin $Fe^{II}$. No identifiable peaks were found in the mass spectra, however it is strongly suspected that even ESI, which is considered to be a 'soft' ionisation techinque, is too damaging to the complex (in fact the same was true for other complexes which are not mentioned in this report).

The higher potential for the E($Fe^{III}/Fe^{II}$) redox couple in **FeLPI** compared to **FeLBI** means that **FeLPI** is more stable to oxidation by ~100 eV. This is a logical observation as the greater degree of delocalisation across the phenanthroline compared to the bipyridine causes the ligand to be less electron-donating to the $Fe^{II}$ centre through the nitrogen atoms. The reduction processes at -1.20 and -1.24 V for FeLPI and FeLBI respectively are likely to be the E($Fe^{II}/Fe^{I}$) redox couples, but EPR after bulk electrolysis is required to confirm this. These

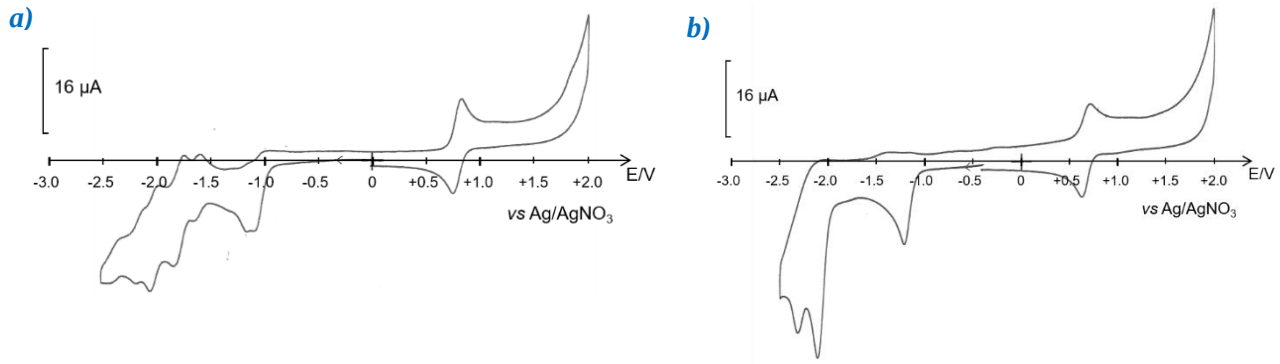


***Figure 28:*** *Cyclic voltammograms of 0.5 mM **FeLPI** (a) and **FeLBI** (b) in MeCN + 0.1 M [Bu4N]BF4.*

potentials also differ but to a lesser extent than the oxidation potentials because the donor effect of the ligand increases the energy of the metal HOMO more than the LUMO. The potentials suggest that the complexes could be reduced by **TATA**$^{\bullet}$. However, both processes have a very small degree of reversibility, if any. Although it is unlikely, this is not to say that the complexes could not be used in catalysis; under photocatalytic conditions the process may be more reversible.

[**Fe(LPI)Cl$_2$**] was obtained as a green solid after heating **LPI** in butanol with anhydrous $FeCl_2$ overnight. Evidence for [**Fe(LPI)Cl$_2$**] was seen in peaks found for $[M - Cl]^+$ and $[M - 2Cl]^{2+}$ in the mass spectrum (Fig 29a). [**Fe(LPI)Cl$_2$**] is less stable than **FeLPI** and **FeLBI** to oxidation to $Fe^{III}$ in air as the process occurs at -0.30 V, but the process seems reversible (Fig. 29b). The lower potential can be attributed to the strong electon-donating nature of the chloride ligands. The same reasoning also explains the lower potential of the $E(Fe^{II}/Fe^{I})$ redox couple which occurs at -1.24 V (-0.94 V *vs* SCE). This process has a high degree of reversibility and therefore suggests that it could be used in conjugation with **TATA**$^+$. The CV also exhibits a reversible process for the $E(Fe^{IV}/Fe^{III})$ redox couple at +1.13 V and an irreversible process for the oxidation of $Cl^-$ at +0.38 V.

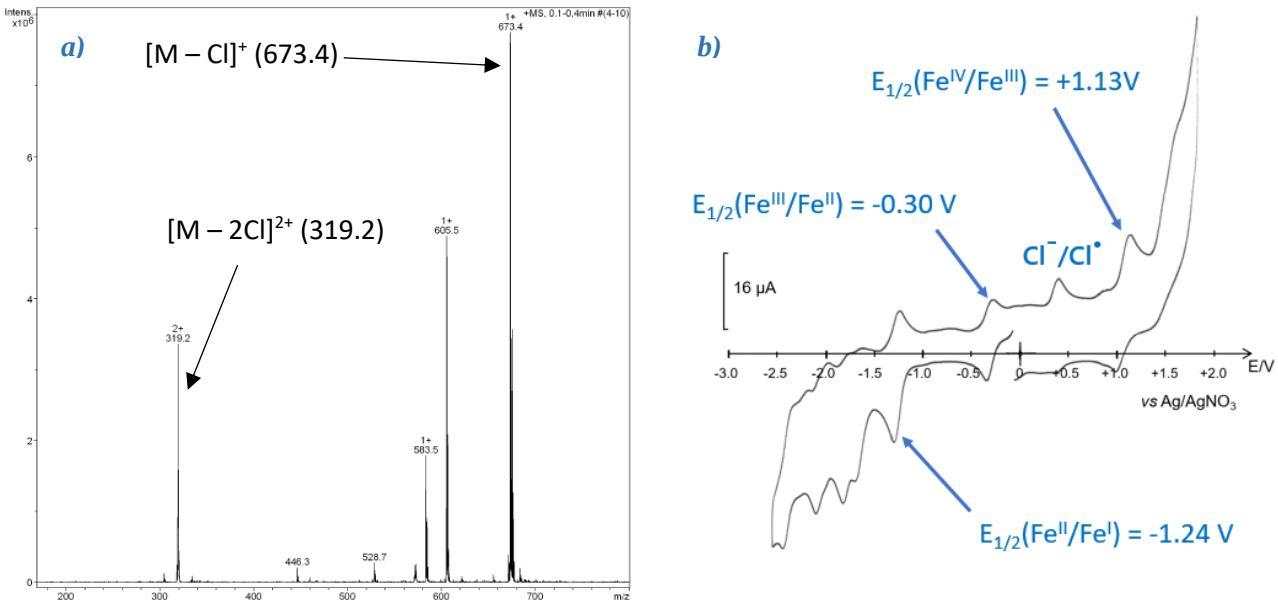


***Figure 29:*** *a) Mass spectrum of **[Fe(LPI)Cl$_2$]**; b) Cyclic voltammogram of 0.5 mM **[Fe(LPI)Cl$_2$]** in MeCN + 0.1 M [Bu4N]BF4 showing the hypothesised redox processes.*

The poor solubility of all four complexes in water means that they would need to be modified before photocatalytic tests for proton reduction in aqueous media can be carried out. For example, water-solubilising groups, such as an ammonium cation, could be incorporated onto the phenyl groups. However, the photocatalytic reduction of $CO_2$ is usually performed in acetonitrile and these complexes have excellent solubility in acetonitrile. Given the resemblance to the Co and Fe quaterpyridine complexes, these complexes may have potential applications in photocatalytic reduction of $CO_2$.

# *V) Conclusion*

This project has been devoted to the synthesis and study of three-component systems for the photocatalytic production of $H_2$ via proton reduction that do not contain precious metals. $H_2$ could potentially be the renewable fuel of the future, so it is important to develop new methods of producing $H_2$ that do not use up valuable and diminishing resources.

The first section of the project saw the investigation of the use of a novel organic dye, the triazatriangulenium cation **TATA$^+$**, as a photosensitizer. Efficient proton reduction has been demonstrated with many precious metal photosensitizers based around ruthenium or idiuium, however these complexes often suffer from poor stability in aqueous media. As far as organic dyes are concerned, there are few families which have been employed as photosensitizers and efficicent proton reduction in these systems is yet to be achieved. These dyes can typically only operate in a mixed aqueous/organic media due to poor solubility and stability in water and all suffer from decomposition from their reduced radical state which is formed by reductive quenching. Unlike nearly all other organic dyes, **TATA$^+$** is soluble and stable in a fully aqueous media. Reported in this work is the efficicent generation of $H_2$ using **TATA$^+$** as a photosensitizer, $[Co^{III}(CR)(H_2O)_2]^{3+}$ as a catalyst and ascorbate as a sacrificial electron donor in a completely precious metal-free system. Importantly, this system is most efficient under acidic conditions (pH 4.5) which is preferential for the reduction of protons. The high activity of **TATA$^+$** can be attributed to the stabilizing delocalization of the radical formed in the reduced state and the presence of three electron-donating nitrogen donors. The most ideal concentrations of the photosensitizer and catalyst were determined and found to be 250 μM and 10 μM respectively, at which turn-over-numbers over 4000 were achieved. The turn-over-numbers achieved by this system are unparalled among those achieved by other organic photosensitizers and even the prototypical photosensitizer $[Ru(bpy)_3]^{2+}$. More work is needed to determine the reason for the decrease in activity at concentrations greater than 250 μM. Moreover, slight decomposition of **TATA$^+$** is observed and future work needs to be carried out to discover the origin of this decomposition. This could be done by isolating the decomposition product at the end of the photocatalysis for analysis. There is also the potential to increase the performance of this system by covalently linking **TATA$^+$** to **14PDN** in a dyad. Although the PS/Cat ratio in dyads cannot be optimised, they have been found to have increased performances over non-linked systems due to the proximity of the two species and therefore the increased rate of electron transfer. New experimental procedures also need to be developed to ensure reproducibility and eleviate discrepancy between sets of experimental data with the same conditions.

This project has also seen the development of new cobalt/iron complexes as potential $H_2$-evolving catalysts. Phenanthroline and bipyridine (bis)imine ligands were synthesised and used for their ability to stabilise the M(I) species formed during the catalytic cycle via electron delocalization across the pyridine-imine moieties. These complexes took inspiration from $[Co^{III}(CR)(H_2O)_2]^{3+}$ and cobalt/iron quaterpyridine complexes which have been shown to be efficicent $H_2$-evolving catalysts. Four complexes have been reported in this work. $[Co(LPI)(MeCN)_2](BF_4)_2$ was synthesised in high yield and found to have several reversible redox processes. EPR was used to help assign these processes and determine that $E(Co^{II}/Co^{I})$ = -1.45 V (*vs* SCE). This low potential suggests that $[Co(LPI)(MeCN)_2](BF_4)_2$ would not be a compatible catalyst with **TATA$^+$** but may be compatible with $[Ru(bpy)_3]^{2+}$. Three iron complexes, $[Fe(LPI)(EtOH)_2](BF_4)_2$, $[Fe(LBI)(EtOH)_2](BF_4)_2$ and $[Fe(LPI)Cl_2]$ were synthesised. The former two complexes displayed reduction potentials of -0.77 V and -0.90 V (*vs* SCE) respectively for the $E(Fe^{II}/Fe^{I})$ redox couple. Whilst these are ideal potentials for a $H_2$-evolving catalyst, the processes appear to be almost completely irreversible. The latter complex displayed a reversible redution process for the same redox couple at -0.94 V (*vs* SCE) which suggests that it could potentially be used as a $H_2$-evolving catalyst with **TATA$^+$**. However, time restraints on the project prevented the testing of these complexes in photocatalysis. As such, there is plenty of future work to be done with these complexes. Full characterization of the complexes is needed (crystal structure, EPR, etc…) as well as photocatalytic tests for the reduction of protons and $CO_2$. All of the complexes need to be modified to increase water solubility. Futhermore, complexation to other first-row transition metals (such as nickel or manganese) could be attemped as well as modifications to the ligands. This work has barely scratched the surface in terms of the potential applications of this genre of complexes as $H_2$-evolving catalysts.

# *VI) Appendix (Supporting Information)*

***Table S1:*** *Photocatalysis data. Total solutions made up to 5 mL with 0.1 M $HA^-/H_2A$ and 1.0 M acetate buffer (pH 4.5). Irradiation 700 – 400 nm for 21 h.*

| [**TATA$^+$**] / µM | [**14PDN**] / µM | PS:Cat | Initial A | Final A | Decomposition of **TATA$^+$** / % | $V_{H2}$ / mL | TON |
|---|---|---|---|---|---|---|---|
| 100 | 10 | 10:1 | 0.089 | 0.045 | 49.4 % | 3.09 | 2530 |
| 100 | 10 | 10:1 | 0.090 | 0.032 | 64.4 % | 3.52 | 2880 |
| 250 | 10 | 25:1 | - | - | - | 4.94 | 4042 |
| 250 | 10 | 25:1 | 0.221 | 0.094 | 57.5 % | 5.04 | 4121 |
| 250 | 5 | 50:1 | 0.220 | 0.098 | 55.5 % | 2.44 | 3984 |
| 250 | 5 | 50:1 | - | - | - | 2.48 | 4064 |
| 250 | 2.5 | 100:1 | 0.220 | 0.110 | 50.0 % | 1.52 | 4967 |
| 250 | 2.5 | 100:1 | - | - | - | 1.55 | 5073 |
| 250 | 1 | 250:1 | - | - | - | 0.71 | 5777 |
| 250 | 1 | 250:1 | - | - | - | 0.75 | 6176 |
| 500 | 10 | 50:1 | 0.440 | 0.252 | 42.7 % | 3.41 | 2793 |
| 500 | 10 | 50:1 | 0.440 | 0.283 | 35.7 % | 3.55 | 2900 |
| 1000 | 10 | 100:1 | 0.878 | 0.599 | 31.8 % | 2.61 | 2132 |
| 1000 | 10 | 100:1 | 0.875 | 0.640 | 26.9 % | 2.66 | 2180 |

***Table S2:*** *GC calibration data used to plot Fig. S1.*

| 1.045 % $H_2$ | 4.965 % $H_2$ |
|---|---|
| 2.00 | 9.73 |
| 2.00 | 9.88 |
| 2.00 | 9.86 |
| 2.07 | 9.78 |
| 2.06 | 9.97 |
| 2.09 | 9.91 |
| 2.09 | 9.70 |
| 2.03 | 9.94 |
| 2.05 | 9.90 |
| 2.11 | - |

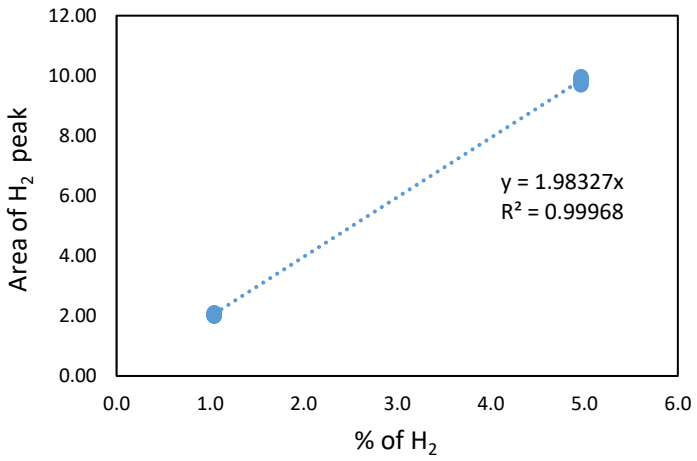


***Figure S1:*** *Plot of the area of $H_2$ peak in the GC spectrum vs % of $H_2$ used for internal calibration of photocatalysis experiments.*

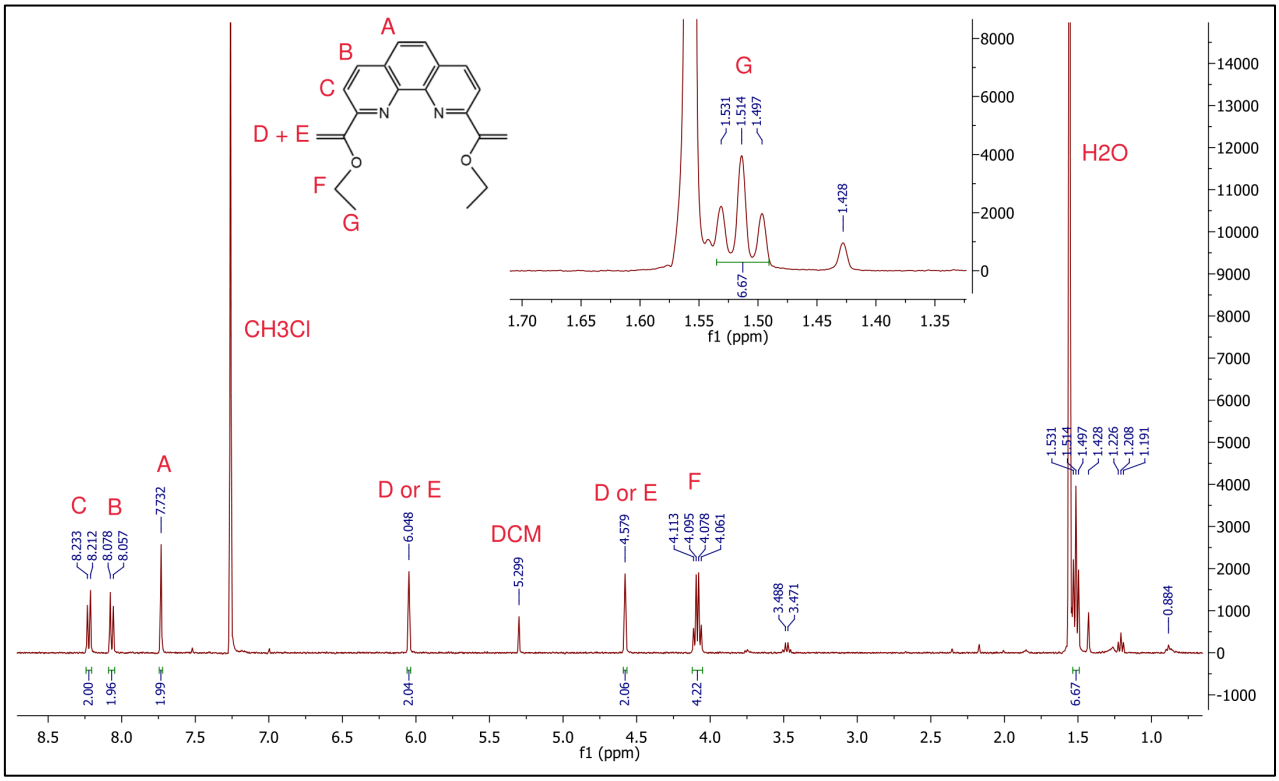


***Figure S2:*** *$^{1}$H NMR spectrum (400 MHz) of the ethoxy-vinyl intermediate of* ***L1*** *in $CDCl_3$.*

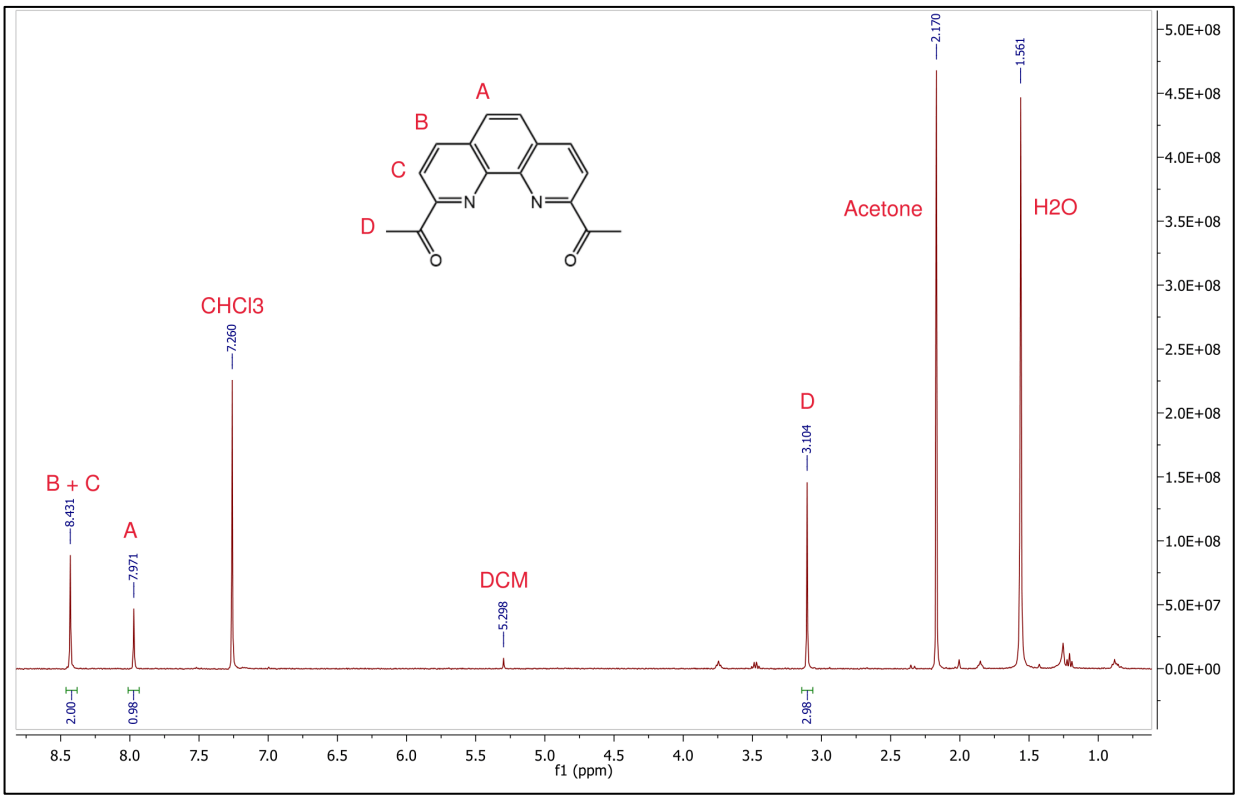


***Figure S3:*** *$^{1}$H NMR spectrum (400 MHz) of* ***L1*** *in $CDCl_3$.*

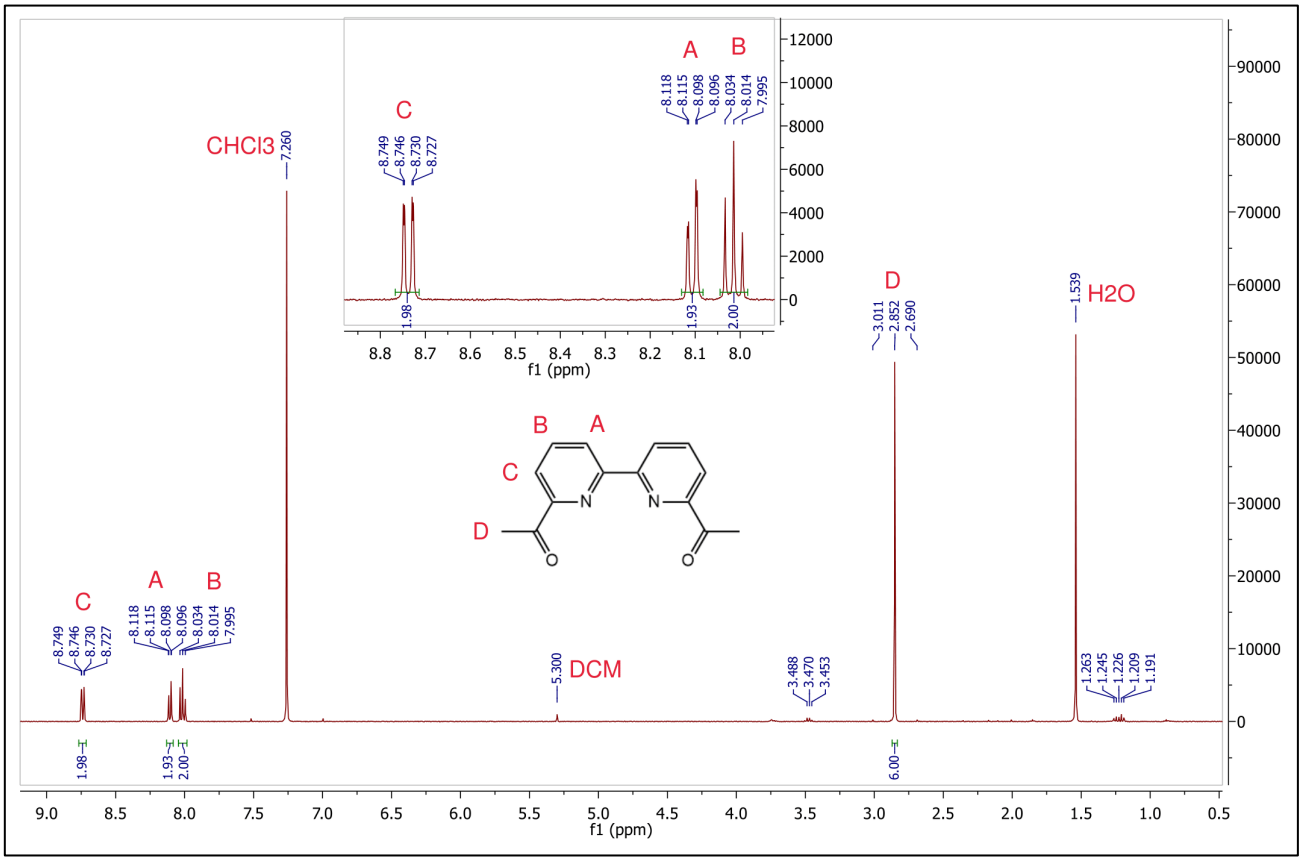


***Figure S4:*** *$^{1}$H NMR spectrum (400 MHz) of* ***L2*** *in $CDCl_3$.*

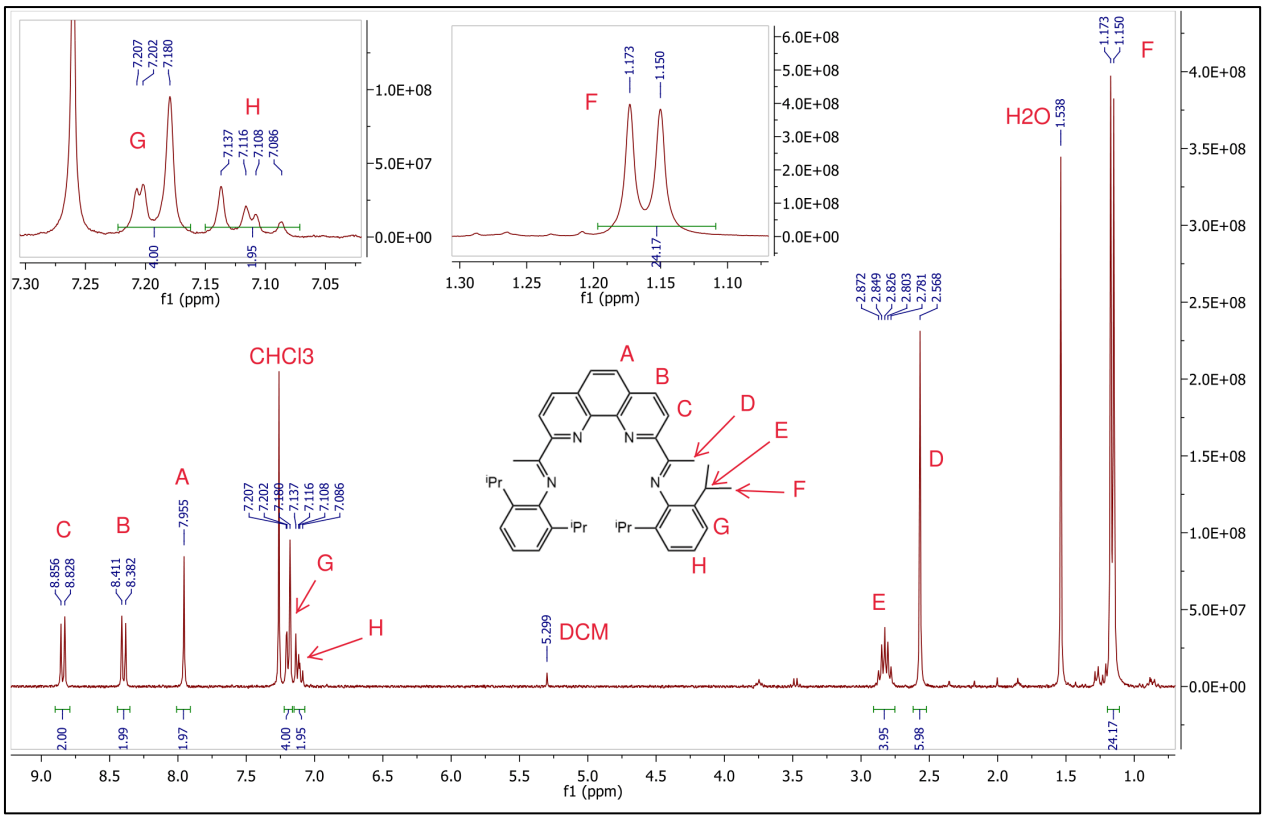


***Figure S5:*** *$^{1}$H NMR spectrum (300 MHz) of* ***LPI*** *in $CDCl_3$.*

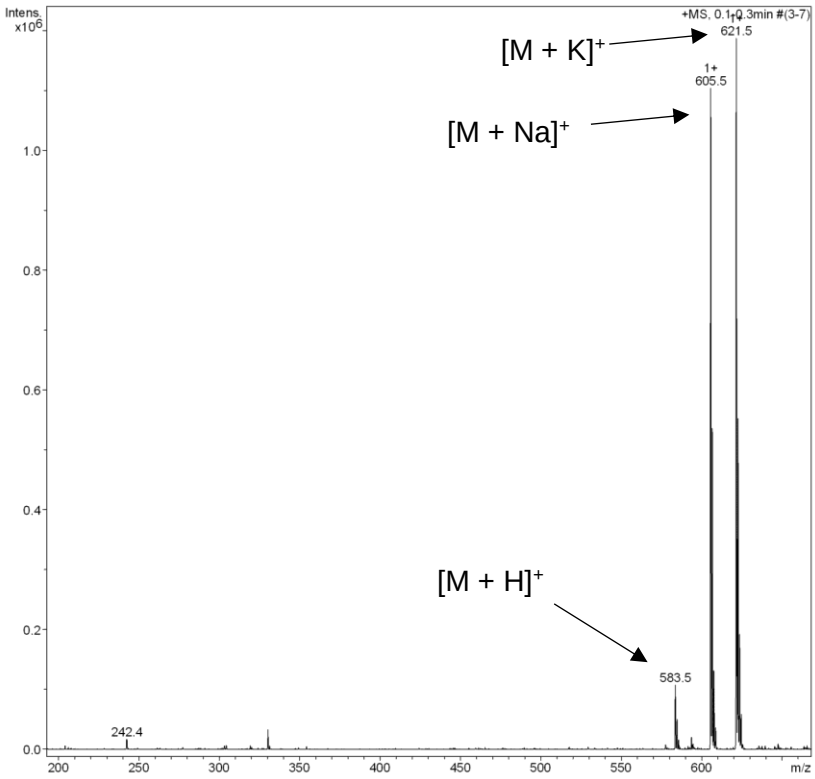


***Figure S6:*** *Mass spectrum (ESI) of* ***LPI****.*

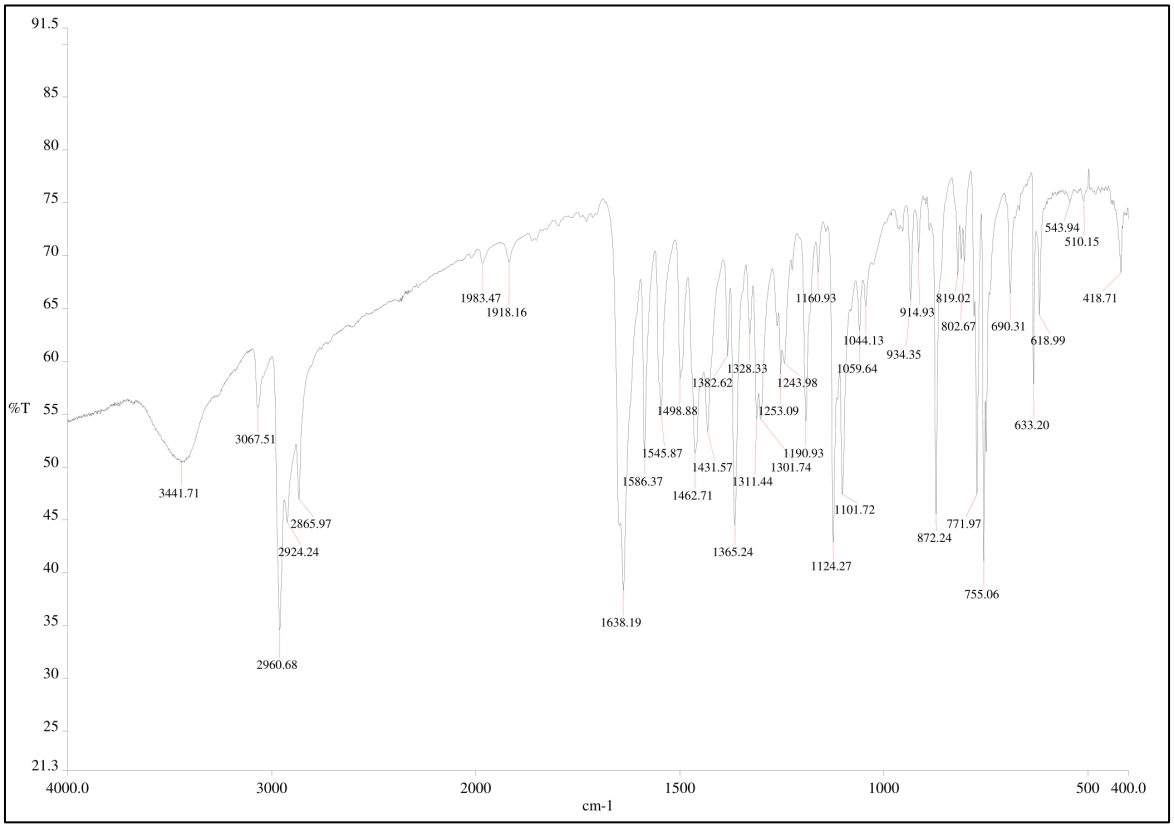


***Figure S7:*** *IR spectrum of* ***LPI*** *(KBr tablet).*

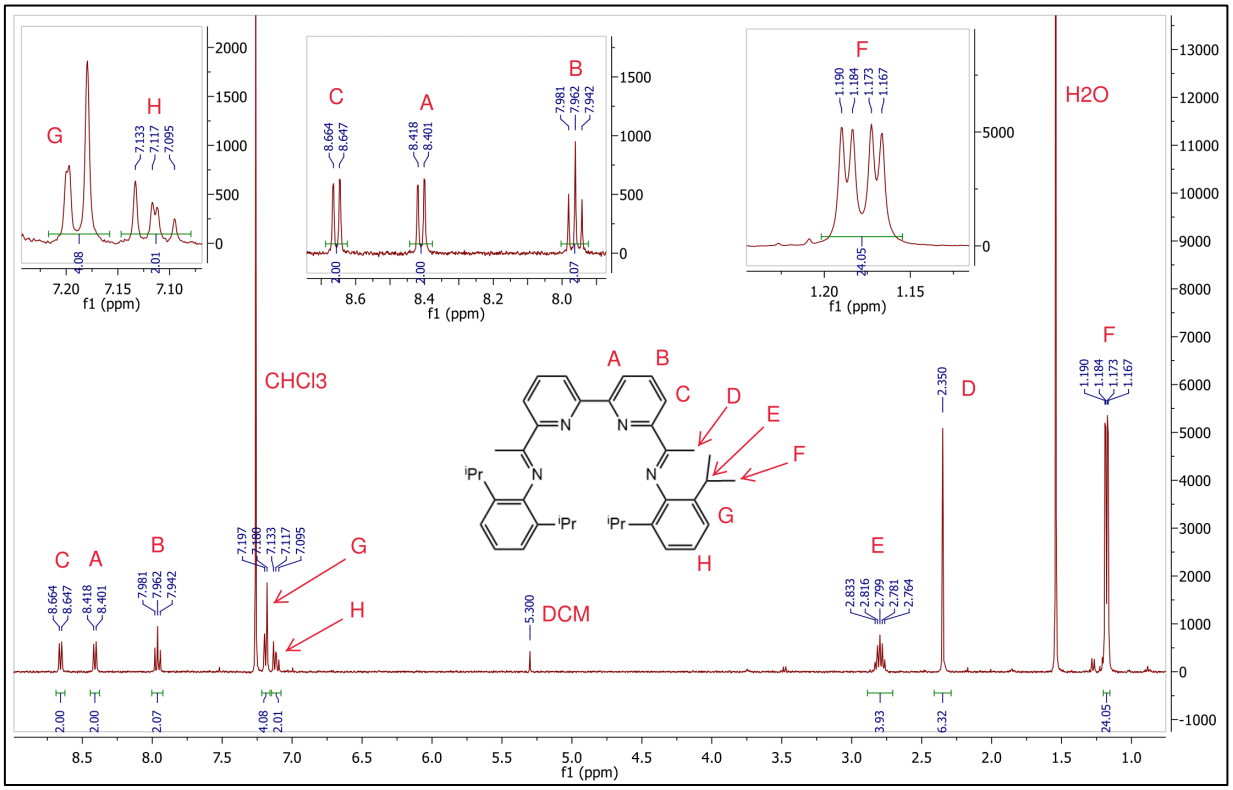


***Figure S8:*** *$^{1}$H NMR spectrum (400 MHz) of* ***LBI*** *in $CDCl_3$.*

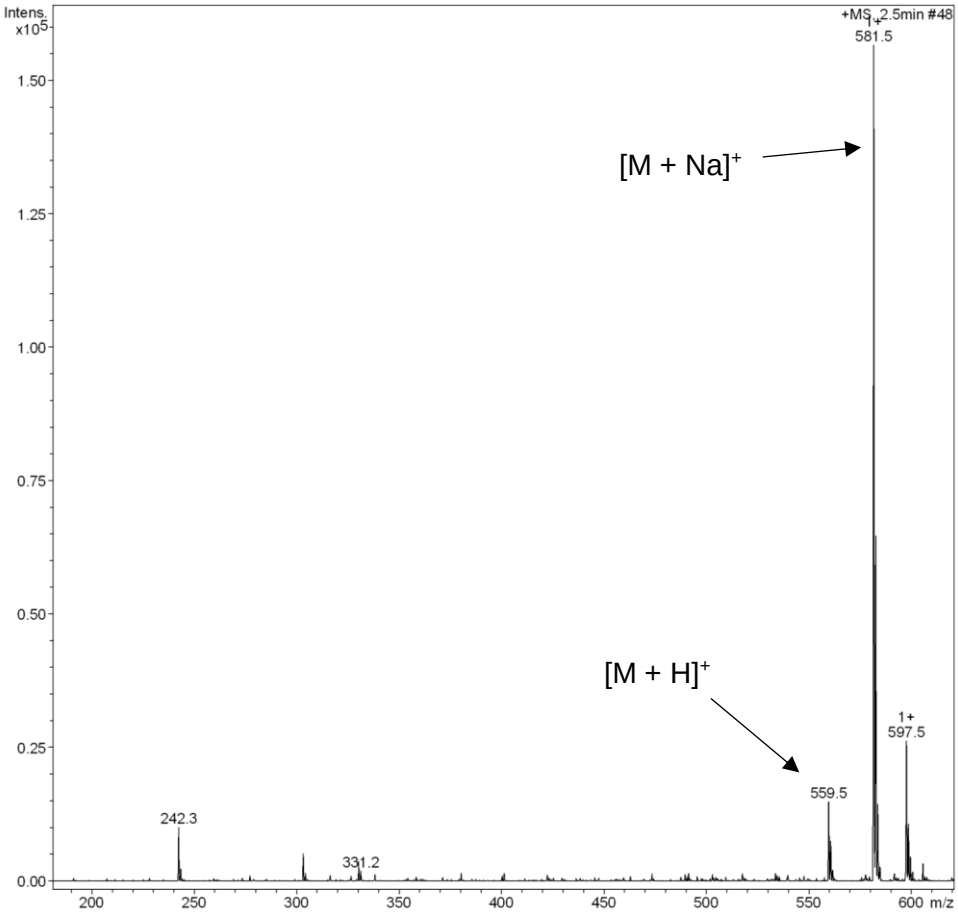


***Figure S9:*** *Mass spectrum (ESI) of* ***LBI****.*

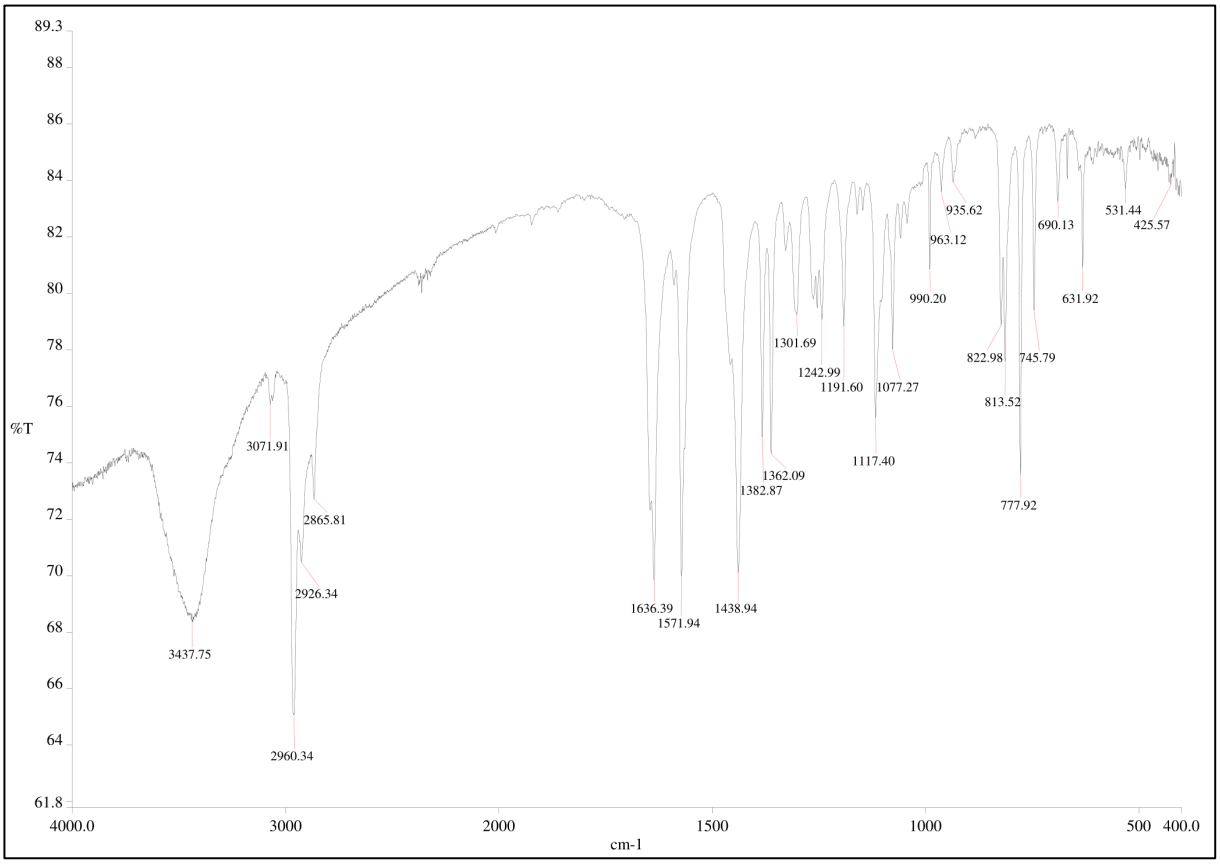


***Figure S10:*** *IR spectrum of* ***LBI*** *(KBr tablet).*

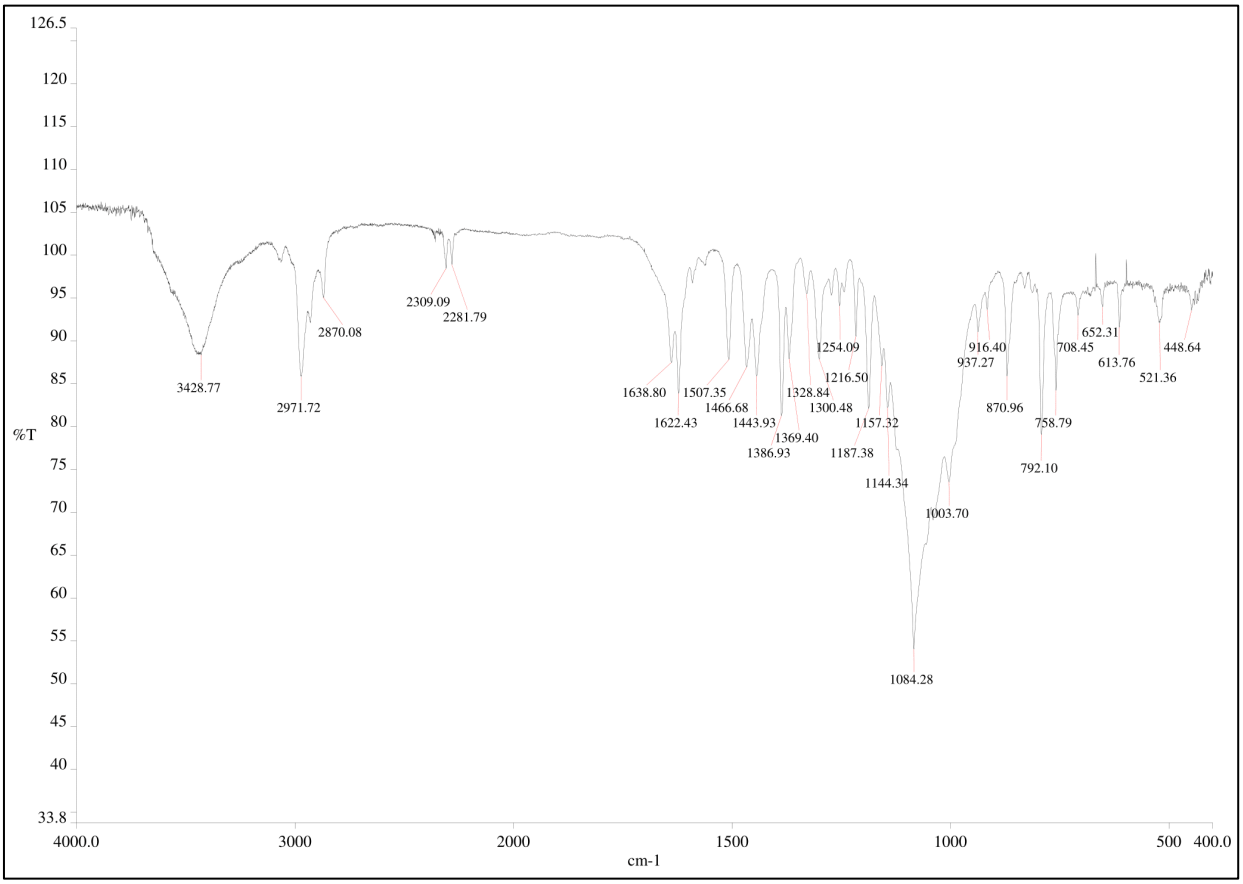


***Figure S11:*** *IR spectrum of* ***CoLPI*** *(KBr tablet).*

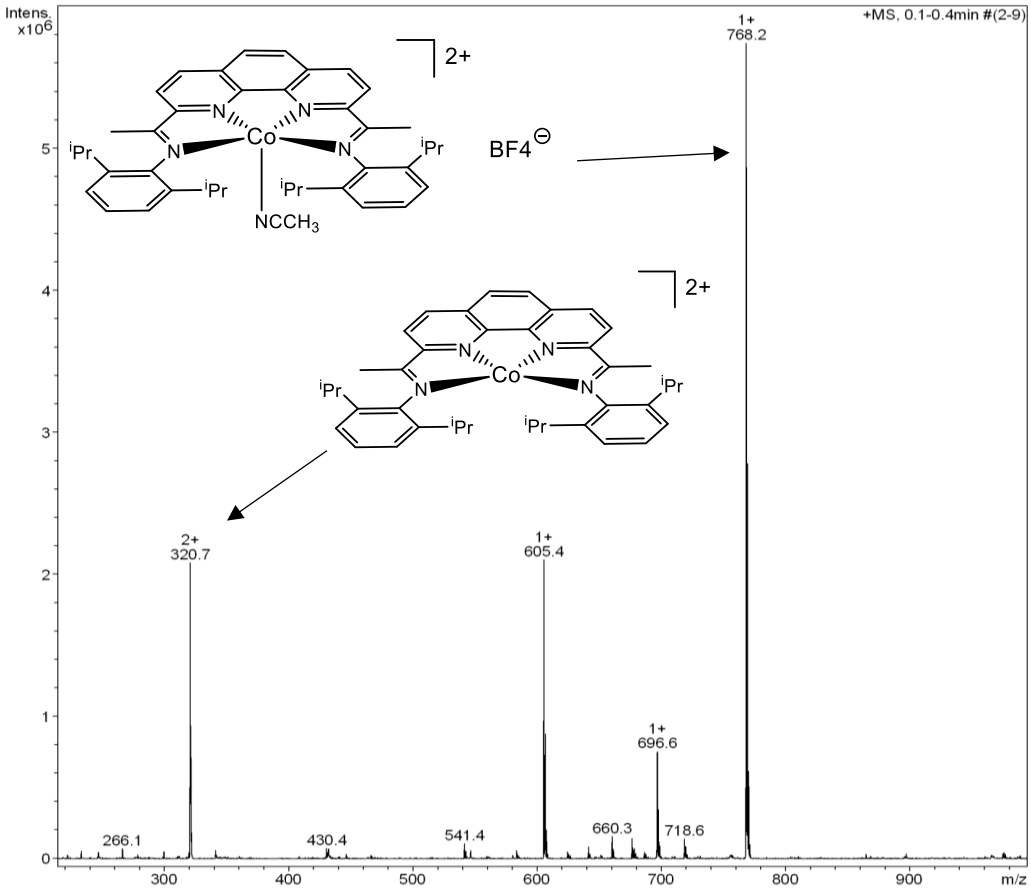


***Figure S12:*** *Mass Spectrum (ESI) of CoLPI.*

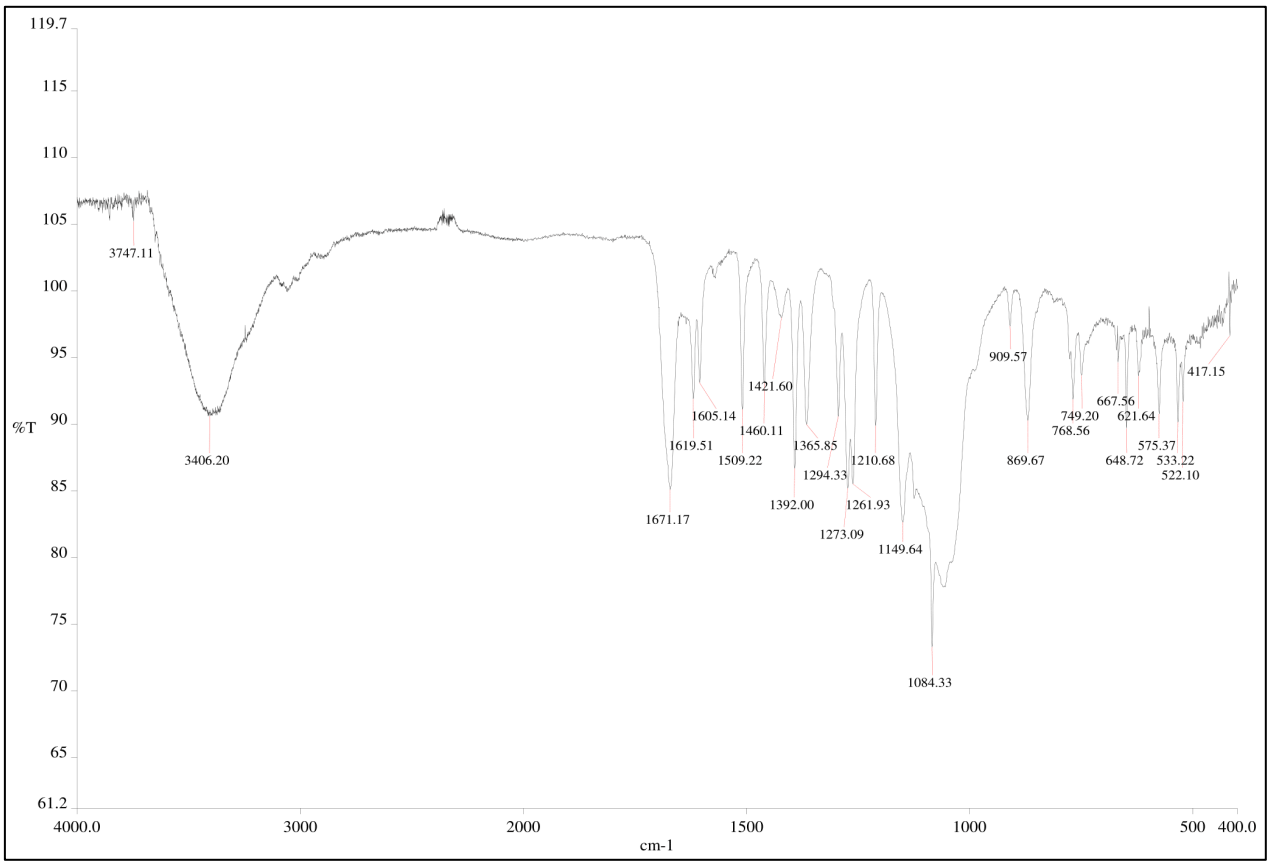


***Figure S13:*** *IR spectrum of* ***FeLPI*** *(KBr tablet).*

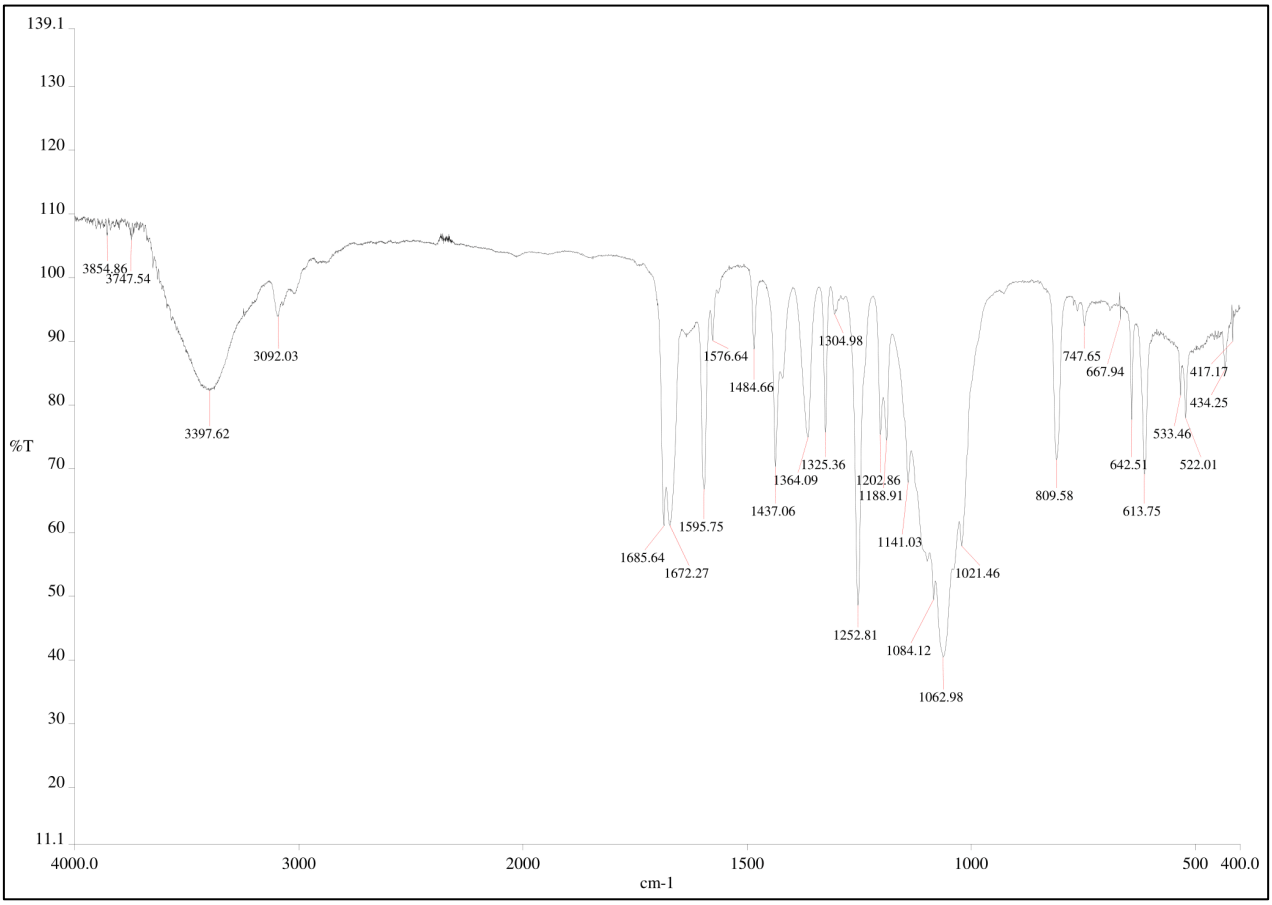


***Figure S14:*** *IR spectrum of* ***FeLBI*** *(KBr tablet).*

## *Reference List*


1 N. Armaroli and V. Balzani, *ChemSusChem*, 2011, **4**, 21–36.

2 J. N. D. Arthur W. Adamson, *J. Am. Chem. Soc.*, 1971, **93**, 1800–1801.

3 A. Juris, V. Balzani, F. Barigelletti, S. Campagna, P. Belser and A. von Zelewsky, *Coord. Chem. Rev.*, 1988, **84**, 85–277.

4 X.-H. Wang, S. Goeb, Z.-Q. Ji, N. A. Pogulaichenko and F. N. Castellano, *Inorg. Chem. (Washington, DC, United States)*, 2011, **50**, 705–707.

5 A. Fihri, V. Artero, A. Pereira and M. Fontecave, *Dalt. Trans.*, 2008, 5567–5569.

6 P. Zhang, P. A. Jacques, M. Chavarot-Kerlidou, M. Wang, L. Sun, M. Fontecave and V. Artero, *Inorg. Chem.*, 2012, **51**, 2115–2120.

7 T. Lazarides, T. McCormick, P. Du, G. Luo, B. Lindley and R. Eisenberg, *J. Am. Chem. Soc.*, 2009, **131**, 9192–9194.

8 T. M. McCormick, B. D. Calitree, A. Orchard, N. D. Kraut, F. V. Bright, M. R. Detty and R. Eisenberg, *J. Am. Chem. Soc.*, 2010, **132**, 15480–15483.

9 T. M. McCormick, Z. Han, D. J. Weinberg, W. W. Brennessel, P. L. Holland and R. Eisenberg, *Inorg. Chem.*, 2011, **50**, 10660–10666.

10 L. Gong, J. Wang, H. Li, L. Wang, J. Zhao and Z. Zhu, *Catal. Commun.*, 2011, **12**, 1099–1103.

11 H.-Q. Zheng, H. Rao, X.-Z. Hu, X.-H. Li, Y.-T. Fan and H.-W. Hou, *Sol. Energy*, 2014, **105**, 648–655.

12 P. Zhang, M. Wang, J. Dong, X. Li, F. Wang, L. Wu and L. Sun, *J. Phys. Chem. C*, 2010, **114**, 15868–15874.

13 F. Lakadamyali, M. Kato, N. M. Muresan and E. Reisner, *Angew. Chemie - Int. Ed.*, 2012, **51**, 9381–9384.

14 F. Wang, W. G. Wang, X. J. Wang, H. Y. Wang, C. H. Tung and L. Z. Wu, *Angew. Chemie - Int. Ed.*, 2011, **50**, 3193–3197.

15 P. Zhang, M. Wang, Y. Na, X. Li, Y. Jiang and L. Sun, *Dalt. Trans.*, 2010, **39**, 1204–1206.

16 H. Y. Wang, W. G. Wang, G. Si, F. Wang, C. H. Tung and L. Z. Wu, *Langmuir*, 2010, **26**, 9766–9771.

17 X. Li, M. Wang, D. Zheng, K. Han, J. Dong and L. Sun, *Energy Environ. Sci.*, 2012, **5**, 8220.

18 C. Orain, F. Quentel and F. Gloaguen, *ChemSusChem*, 2014, **7**, 638–643.

19 T. Sakai, D. Mersch and E. Reisner, *Angew. Chemie - Int. Ed.*, 2013, **52**, 12313–12316.

20 C. L. Hartley, R. J. Dirisio, M. E. Screen, K. J. Mayer and W. R. McNamara, *Inorg. Chem.*, 2016, **55**, 8865–8870.

21 U. J. Kilgore, J. A. S. Roberts, D. H. Pool, A. M. Appel, M. P. Stewart, M. R. Dubois, W. G. Dougherty, W. S. Kassel, R. M. Bullock and D. L. Dubois, *J. Am. Chem. Soc.*, 2011, **133**, 5861–5872.

22 M. Rakowski Dubois and D. L. Dubois, *Acc. Chem. Res.*, 2009, **42**, 1974–1982.

23 M. P. Mclaughlin, T. M. McCormick, R. Eisenberg, L. Patrick and P. L. Holland, *Chem. Commun.*, 2011, **47**, 7989.

24 A. Das, Z. Han, W. W. Brennessel, P. L. Holland and R. Eisenberg, *ACS Catal.*, 2015, **5**, 1397–1406.

25 Z. Han, L. Shen, W. W. Brennessel, P. L. Holland and R. Eisenberg, *J. Am. Chem. Soc.*, 2013, **135**, 14659–14669.

26 Z. Han, W. R. McNamara, M. S. Eum, P. L. Holland and R. Eisenberg, *Angew. Chemie - Int. Ed.*, 2012, **51**, 1667–1670.

27 H. Rao, W.-Q. Yu, H.-Q. Zheng, J. Bonin, Y.-T. Fan and H.-W. Hou, *J. Power Sources*, 2016, **324**, 253–260.

28 X. Song, H. Wen, C. Ma, H. Chen and C. Chen, *New J. Chem.*, 2015, **39**, 1734–1741.

29 H. Cui, J. Wang, M. Hu, C. Ma, H. Wen, X. Song and C. Chen, *Dalton Trans.*, 2013, **42**, 8684–91.

30 H. Rao, Z.-Y. Wang, H.-Q. Zheng, X.-B. Wang, C.-M. Pan, Y. Fan and H. Hou, *Catal. Sci. Technol.*, 2015, **5**.

31 P. H. A. Kankanamalage, S. Mazumder, V. Tiwari, K. K. Kpogo, H. B. Schlegel and N. Verani, *Chem. Commun.*, 2016, **52**, 13357–13360.

32 S. Roy, M. Bacchi, G. Berggren and V. Artero, *ChemSusChem*, 2015, **8**, 3632–3638.

33 A. J. Esswein, D. G. Nocera, A. J. Esswein and D. G. Nocera, *Chem. Rev.*, 2007, **107**, 4022–4047.

34 D. Gust, T. A. Moore and A. L. Moore, *Acc. Chem. Res.*, 2009, **42**, 1890–1898.

35 Y. Pellegrin and F. Odobel, *Comptes Rendus Chim.*, , DOI:10.1016/j.crci.2015.11.026.

36 M. Guttentag, A. Rodenberg, C. Bachmann, A. Senn, P. Hamm and R. Alberto, *Dalton Trans.*, 2013, **42**, 334–7.

37 M. Guttentag, A. Rodenberg, R. Kopelent, B. Probst, C. Buchwalder, M. Brandstätter, P. Hamm and R. Alberto, *Eur. J. Inorg. Chem.*, 2012, 59–64.

38 W. M. Singh, T. Baine, S. Kudo, S. Tian, X. A. N. Ma, H. Zhou, N. J. Deyonker, T. C. Pham, J. C. Bollinger, D. L. Baker, B. Yan, C. E. Webster and X. Zhao, *Angew. Chemie - Int. Ed.*, 2012, **51**, 5941–5944.

39 N. Sutin, C. Creutz and E. Fujita, *Comments Inorg. Chem.*, 1997, **19**, 67–92.

40 T. Stoll, M. Gennari, I. Serrano, J. Fortage, J. Chauvin, F. Odobel, M. Rebarz, O. Poizat, M. Sliwa, A. Deronzier and M. N. Collomb, *Chem. - A Eur. J.*, 2013, **19**, 782–792.

41 H. Ozawa, Y. Yokoyama, M. Haga and K. Sakai, *Dalt. Trans.*, 2007, 1197–1206.

42 G. F. Manbeck and K. J. Brewer, *Coord. Chem. Rev.*, 2013, **257**, 1660–1675.

43 S. Fukuzumi, T. Kobayashi and T. Suenobu, *Angew. Chemie - Int. Ed.*, 2011, **50**, 728–731.

44 T. Stoll, M. Gennari, J. Fortage, C. E. Castillo, M. Rebarz, M. Sliwa, O. Poizat, F. Odobel, A. Deronzier and M. N. Collomb, *Angew. Chemie - Int. Ed.*, 2014, **53**, 1654–1658.

45 R. Gueret, C. E. Castillo, M. Rebarz, F. Thomas, A. A. Hargrove, J. P??caut, M. Sliwa, J. Fortage and M. N. Collomb, *J. Photochem. Photobiol. B Biol.*, 2015, **152**, 82–94.

46 Z. Guo, S. Cheng, C. Cometto, E. Anxolabehere-Mallart, S. M. Ng, C. C. Ko, G. Liu, L. Chen, M. Robert and T. C. Lau, *J. Am. Chem. Soc.*, 2016, **138**, 9413–9416.

47 K. Sakai and H. Ozawa, *Coord. Chem. Rev.*, 2007, **251**, 2753–2766.

48 E. Deponti, A. Luisa, M. Natali, E. Iengo and F. Scandola, *Dalton Trans.*, 2014, **43**, 16345–16353.

49 B. Probst, C. Kolano, P. Hamm and R. Alberto, *Inorg. Chem.*, 2009, **48**, 1836--1843.

50 J. I. Goldsmith, W. R. Hudson, M. S. Lowry, T. H. Anderson and S. Bernhard, *J. Am. Chem. Soc.*, 2005, **127**, 7502–7510.

51 M. S. Lowry, J. I. Goldsmith, J. D. Slinker, R. a Pascal, G. G. Malliaras, S. Bernhard and R. Rohl, *J. Mater.*, 2005, **17**, 5712–5719.

52 G.-G. Luo, K. Fang, J.-H. Wu, J.-C. Dai and Q.-H. Zhao, *Phys. Chem. Chem. Phys.*, 2014, **16**, 23884–23894.

53 R. P. Sabatini, B. Lindley, T. M. McCormick, T. Lazarides, W. W. Brennessel, D. W. McCamant and R. Eisenberg, *J. Phys. Chem. B*, 2016, **120**, 527–534.

54 G.-G. Luo, K. Fang, J. Wu and J. Mo, *Chem. Commun.*, 2015, **51**.

55 D. Adams, M. Nolan, J. J. Walsh, L. Mears, A. J. Cowan, E. Draper, B. Dietrich, M. Wallace, M. Barrow and S. M. King, *J. Mater. Chem. A*, 2017, **5**, 7555–7563.

56 S. Varma, C. E. Castillo, T. Stoll, J. Fortage, A. G. Blackman, F. Molton, A. Deronzier and M.-N. Collomb, *Phys. Chem. Chem. Phys.*, 2013, **15**, 17544–52.

57 E. Reisner, *Eur. J. Inorg. Chem.*, 2011, 1005–1016.

58 S. I. Allakhverdiev, V. Thavasi, V. D. Kreslavski, S. K. Zharmukhamedov, V. V. Klimov, S. Ramakrishna, D. A. Los, M. Mimuro, H. Nishihara and R. Carpentier, *J. Photochem. Photobiol. C Photochem. Rev.*, 2010, **11**, 101–113.

59 W. Zhang, J. Hong, J. Zheng, Z. Huang and R. Xu, *Elements*, 2011, 2–5.

60 M. Nippe, R. S. Khnayzer, J. A. Panetier, D. Z. Zee, B. S. Olaiya, M. Head-Gordon, C. J. Chang, F. N. Castellano and J. R. Long, *Chem. Sci.*, 2013, **4**, 3934.

61 M. Natali, A. Luisa, E. Iengo and F. Scandola, *Chem. Commun. (Camb).*, 2014, **50**, 1842–4.

62 M. Vennampalli, G. Liang, L. Katta, C. E. Webster and X. Zhao, *Inorg. Chem.*, 2014, **53**, 10094–10100.

63 R. S. Khnayzer, V. S. Thoi, M. Nippe, A. E. King, J. W. Jurss, K. A. El Roz, J. R. Long, C. J. Chang and F. N. Castellano, *Energy Environ. Sci.*, 2014, **7**, 1477–1488.

64 C.-F. Leung, S.-M. Ng, C.-C. Ko, W.-L. Man, J. Wu, L. Chen and T.-C. Lau, *Energy Environ. Sci.*, 2012, **5**, 7903.

65 U. J. Kilgore, M. P. Stewart, M. L. Helm, W. G. Dougherty, W. S. Kassel, M. R. Dubois, D. L. Dubois and R. M. Bullock, *Inorg. Chem.*, 2011, **50**, 10908–10918.

66 G. a Griffith, M. J. Al-Khatib, K. Patel, K. Singh and G. a Solan, *Dalton Trans.*, 2009, **2**, 185–196.

67 L. Wang, W. Sun, L. Han, H. Yang and Y. Hu, *J. Organomet. Chem.*, 2002, **658**, 62–70.

68 J. V Caspar and T. J. Meyer, *J. Am. Chem. Soc.*, 1983, **3**, 5583–5590.

69 W. K. C. Lo, C. E. Castillo, R. Gueret, J. Fortage, M. Rebarz, M. Sliwa, F. Thomas, C. J. McAdam, G. B. Jameson, D. A. McMorran, J. D. Crowley, M.-N. Collomb and A. G. Blackman, *Inorg. Chem.*, 2016, **55**, 4564–4581.

70 D. S. Miller, A. J. Bard, G. Mclendon and J. Fergusont, *J. Am. Chem. Soc.*, 1981, **103**, 5336–5341.

71 L. L. Tinker, N. D. McDaniel, P. N. Curtin, C. K. Smith, M. J. Ireland and S. Bernhard, *Chem. - A Eur. J.*, 2007, **13**, 8726–8732.

72 K. T. Potts, K. a. G. Raiford and M. Keshavarz-K, *J. Am. Chem. Soc.*, 1993, **115**, 2793–2807.

73 R. Zong, D. Wang, R. Hammitt and R. P. Thummel, *J. Org. Chem.*, 2006, **71**, 167–175.

74 W. E. Buschmann and J. S. Miller, *Chem. Eur. J.*, 1998, 1731–1737.

75 M. Ghosh, T. Weyhermüller and K. Wieghardt, *Dalt. Trans.*, 2010, **39**, 1996–2007.